

MOUNTAIN-PLAINS CONSORTIUM

MPC 17-325 | Y. J. Kim

Performance of Steel Girders Repaired with Advanced Composite Sheets in a Corrosive Environment



A University Transportation Center sponsored by the U.S. Department of Transportation serving the Mountain-Plains Region. Consortium members:

Colorado State University
North Dakota State University
South Dakota State University

University of Colorado Denver
University of Denver
University of Utah

Utah State University
University of Wyoming

**PERFORMANCE OF STEEL GIRDERS REPAIRED WITH
ADVANCED COMPOSITE SHEETS IN A CORROSIVE ENVIRONMENT**

Yail Jimmy Kim, Ph.D., P.Eng., FACI
Department of Civil Engineering
University of Colorado Denver
Denver, Colorado

June 2017

Acknowledgments

The principal investigator gratefully acknowledges all individuals who contributed to the present research report.

Disclaimer

The contents of this report reflect the work of the author, who is responsible for the facts and the accuracy of the information presented. This document is disseminated under the sponsorship of the Mountain-Plains Consortium in the interest of information exchange. The U.S. Government assumes no liability for the contents or use thereof.

NDSU does not discriminate in its programs and activities on the basis of age, color, gender expression/identity, genetic information, marital status, national origin, participation in lawful off-campus activity, physical or mental disability, pregnancy, public assistance status, race, religion, sex, sexual orientation, spousal relationship to current employee, or veteran status, as applicable. Direct inquiries to Vice Provost for Title IX/ADA Coordinator, Old Main 201, NDSU Main Campus, 701-231-7708, ndsuoaa.ndsu.edu.

EXECUTIVE SUMMARY

This report presents a two-phase research program studying i) galvanic current influencing deterioration of carbon fiber reinforced polymer (CFRP) sheets bonded to a steel substrate and ii) electrochemical reaction for steel beams strengthened with CFRP.

The first phase of the research presents an experimental program investigating the effect of galvanic current on the physical and mechanical characteristics of CFRP composite sheets bonded to a steel substrate. Electrochemical reaction is induced by galvanic interaction between anodes (CFRP-steel interface specimens) and cathodes (metallic strips) linked with an electrolyte (a 3.5% sodium chloride solution). Thirty-five test specimens are exposed to various periods of galvanic current from 0 to 72 hours until their corrosion rate is converged. Hydrated ferric oxide forms along the CFRP-steel interface with some concentration in the vicinity of its edge, which accompanies a loss in surface area and mass. The electrochemical reaction imposed by the galvanic current exponentially decays with an increase in exposure time. The initiation of corrosion noticeably affects the load-carrying capacity of the CFRP-steel interface, whereas its propagation is not a critical attribute until substantial corrosion damage occurs. CFRP-debonding is the governing failure mode of the interface, irrespective of the degree of galvanic current exposure. The stress-slip behavior of the interface is influenced by the electrochemical reaction and a geometric discontinuity associated with stress singularity. Corrosion-dependent interfacial fracture energy is probabilistically inferred and used for quantifying the degree of interface deterioration subjected to an aggressive corrosion environment.

The second phase of the research discusses the effects of an electrochemical reaction on the physical and chemical responses of steel beams strengthened with carbon fiber reinforced polymer (CFRP) sheets. An accelerated corrosion protocol is used for deteriorating the strengthened beams. Emphasis is placed on the electric potential, mass loss, corrosion current density, corrosion rate, flexural capacity, interfacial strain development, failure mode, and infrared spectroscopy of the beams. Corrosion damage is dispersed with increasing electrochemical reaction time; however, premature CFRP-debonding is not observed. The presence of surface rust tends to impede the flow of electric current and the diffusion of iron ions is reduced, thereby decreasing the rate of corrosion. The consequence of corrosion damage results in a decrease in load-carrying capacity of the strengthened beams along with two phases, such as initiation-propagation and steady-state. The electrochemical effect imposed alters the pattern of CFRP-debonding from discrete-discontinuous to smooth progression. Infrared spectroscopy illustrates that the functional group of the CFRP system changes from a chemistry standpoint as the degree of corrosion augments. Design recommendations are proposed to facilitate the use of CFRP-strengthening for steel members subjected to corrosive service environments.

TABLE OF CONTENTS

PART I: Galvanic Current Influencing Interface Deterioration of CFRP Bonded to a Steel Substrate

1. INTRODUCTION.....	1
2. RESEARCH SIGNIFICANCE.....	3
3. EXPERIMENTAL PROGRAM.....	4
3.1 Specimen Details	4
3.2 Generating Galvanic Current	5
3.3 Post-corrosion Test	6
3.3.1 Physical Properties	6
3.3.2 Mechanical Loading for Residual Capacity	6
4. RESULTS AND DISCUSSION	7
4.1 Formation of Hydrated Ferric Oxide	7
4.2 Corrosion Rate	8
4.3 Interfacial Capacity	8
4.4 Displacement and Strain Response	9
4.5 Bond-slip Behavior	11
5. MODELING OF INTERFACE DETERIORATION	13
5.1 Formulation of Theory	13
5.2 Implementation	14
5.2.1 Fracture Energy	14
5.2.2 Probabilistic Response	15
5.2.3 Interface Deterioration	16
6. SUMMARY AND CONCLUSIONS	18
7. REFERENCES.....	19

PART II: Electrochemical Reaction for Steel Beams Strengthened with CFRP Sheets

8. INTRODUCTION.....	21
9. EXPERIMENTAL PROGRAM.....	22
9.1 Materials	22
9.2 Specimen Preparation	22
9.3 Accelerated Corrosion	23
9.4 Quantification of Corrosion	24
9.5 Efficiency of CFRP-strengthening.....	25
9.6 Flexural Testing and Instrumentation	26
9.7 Fourier Transform Infrared Spectroscopy.....	26

10. TEST RESULTS	27
10.1 Propagation of Corrosion.....	27
10.2 Corrosion Rate	28
10.3 Load-carrying Capacity	29
10.4 Failure Mode.....	30
10.5 Strain Development	31
10.6 Crack Mouth Opening Displacement	32
10.7 Chemical Characterization.....	33
11. DESIGN RECOMMENDATIONS	35
11.1 Equivalent Service Year	35
11.2 Bond Efficiency Factor.....	36
12. SUMMARY AND CONCLUSIONS	38
13. REFERENCES.....	39

LIST OF TABLES

Part I

Table I.1	Mechanical properties	5
Table I.2	Summary of test results.....	5

Part II

Table II.1	Test matrix for CFRP-strengthened beams.....	24
Table II.2	Proposed bond efficiency factor for design	37

LIST OF FIGURES

Part I

Figure I.1	Specimen details: (a) dimension; (b) surface preparation.....	4
Figure I.2	Galvanic current generating protocol for electrochemical reactions: (a) schematic; (b) close-up view of anodes	4
Figure I.3	Post-corrosion monotonic tension test.....	6
Figure I.4	Effect of galvanic current: (a) control: (b) specimens exposed to 36 hours	7
Figure I.5	Variation of physical properties with time: (a) surface area; (b) mass loss.....	7
Figure I.6	Corrosion propagation with time	8
Figure I.7	Interfacial capacity of specimens.....	9
Figure I.8	Failure mode: (a) without galvanic current processing (0 hours); (b) with galvanic current processing (24 hours).....	9
Figure I.9	Load-displacement behavior: (a) 0 hours; (b) 24 hours; (c) 48 hours; (d) 72 hours	10
Figure I.10	Stiffness of the specimens.....	11
Figure I.11	Load-strain behavior: (a) 0 hours; (b) 24 hours; (c) 48 hours.....	11
Figure I.12	Interfacial stress-slip behavior: (a) 0 hours; (b) 24 hours; (c) 48 hours.....	12
Figure I.13	Comparison of maximum local interfacial stresses	12
Figure I.14	Interfacial fracture energy: (a) variation with exposure time; (b) coefficient of variation	14
Figure I.15	Normality check for test specimens.....	15
Figure I.16	Predicted response of interfacial fracture energy: (a) effect of galvanic current exposure time; (b) probability of interface deterioration	16
Figure I.17	Determination of deterioration constant	16
Figure I.18	Deterioration of CFRP-steel interface: (a) progression of deterioration level; (b) development of deterioration rate	17

Part II

Figure II.1	Beam details: (a) dimensions (unit in mm); (b) flexural test and instrumentation	23
Figure II.2	Electrochemical reaction: (a) schematic; (b) test in progress; (c) measuring surface area and mass loss	23
Figure II.3	Fourier transform infrared spectroscopy.....	26
Figure II.4	Propagation of corrosion with time: (a) 12 hours; (b) 36 hours; (c) 72 hours	28
Figure II.5	Consequences of electrochemical reaction: (a) surface area; (b) mass loss; (c) electric potential; (d) corrosion current density.....	28
Figure II.6	Variation of corrosion rate based on Faraday's law	29
Figure II.7	Load-carrying capacity of the beams: (a) ultimate load; (b) efficiency of CFRP-strengthening.....	30
Figure II.8	Load-displacement behavior of CFRP-strengthened beams at various accelerated corrosion periods: (a) 0 hours; (b) 36 hours; (c) 72 hours	30
Figure II.9	Failure mode: (a) ductile fracture cracking; (b) CFRP-debonding.....	31
Figure II.10	CFRP strain development of corroded beams: (a) 12 hours; (b) 36 hours; (c) 72 hours	32
Figure II.11	Strain profile along the CFRP sheet: (a) 12 hours; (b) 36 hours; (c) 72 hours	32
Figure II.12	Crack mouth opening displacement (CMOD) of strengthened beams: (a) up to 36 hours; (b) up to 72 hours	33
Figure II.13	Chemical response of the CFRP sheets: (a) 12 hours; (b) 48 hours; (c) 72 hours	34
Figure II.14	Relationship between accelerated corrosion hour and equivalent service year: (a) predicted corrosion progression on site; (b) predicted corrosion rate on site; (c) proposed corrosion curve for time conversion	36
Figure II.15	Variation of bond efficiency factor.....	36

Part I: Galvanic Current Influencing Interface Deterioration of CFRP Bonded to a Steel Substrate

1. INTRODUCTION

The aging of constructed civil structures is an emerging problem for which the infrastructure community is responsible. In 2013, the Federal Highway Administration of the United States reported that 607,751 bridges are in operation, while 24.3% of them (147,870 bridges) are classified as structurally deficient or functionally obsolete (FHWA 2014). Steel bridges may be deteriorated more than concrete bridges because of their corrosive nature in direct exposure to the environment. The aforementioned FHWA survey supports such a hypothesis: the nation has 191,095 steel and 401,669 concrete bridges, and 38.2% and 16.6% of them are structurally deficient or functionally obsolete, respectively. Typical practices in traditional rehabilitation for corrosion-damaged steel members include the replacement of corroded regions with steel plates by bolting, riveting, or welding (Hollaway and Cadei 2002). This kind of repair may be effective for a limited time because the repair material itself is also susceptible to corrosion, and similar deterioration problems are likely to follow. Rigorous endeavors when dealing with heavy steel plates, including special equipment required for welding and consequent residual stresses, are another issue to be considered. Strengthening deteriorated steel members with carbon fiber reinforced polymer (CFRP) composites is regarded as an alternative to such conventional methods.

CFRP demonstrates favorable density, high tensile strength and modulus, corrosion resistance, and easy manipulation on construction sites (Teng et al. 2012). CFRP sheets may be bonded to a substrate to enhance the behavior of steel members. Epoxy adhesives are predominantly used for civil structure application. The bond between the steel substrate and CFRP is instrumental in preserving the integrity of the interface, while commercially available structural epoxy adhesives have certain minimum durability requirements so that premature cohesion failure of the adhesive may not occur in most cases unless significant environmental distress (e.g., excessive freezing-and-thawing) is imposed. The primary purposes of CFRP strengthening for degraded steel structures are to increase load-carrying capacity, enhance serviceability, and prolong fatigue life (Cadei et al. 2004). Review articles were recently published regarding the state-of-the-art of CFRP-strengthening techniques for steel structures (Zhao and Zhang 2007; Teng et al. 2012; Gholami et al. 2013). The emphasis of these reviews encompasses the importance of surface preparation, bond mechanisms, strengthening methods, failure modes, fatigue resistance, buckling, and environmental durability subjected to temperature, moisture, salted water, and ultraviolet exposure based on existing research results (Smith and Teng 2001; Tao et al. 2007; Shokrieh and Bayat 2007; Egilmez and Yormaz 2011; among others). The issue of galvanic corrosion was briefly mentioned in a few papers (Tavakkolizadeh and Saadatmanesh 2001; Nguyen et al. 2012), which indicates that current knowledge as to the effect of corrosion damage on the performance of CFRP-strengthened steel members is largely limited.

It is well elucidated that interfacial behavior plays a critical role in CFRP strengthening, regardless of substrate materials (e.g., steel or concrete). This is due to stress-sharing between the strengthened structure and the strengthening material (i.e., effectiveness of CFRP rehabilitation) is dependent upon the performance of the interface. Understanding the behavior of the interface subjected to detrimental conditions, either mechanical or environmental, is therefore one of the most salient technical demands in CFRP application (Tavakkolizadeh and Saadatmanesh 2001). Durability aspects for steel members strengthened with CFRP have been reported in recent years at an interface level. Dawood and Rizkalla (2010) conducted a double lap tension test for evaluating the capacity of CFRP-steel interface submerged in a 5% NaCl solution for six months. A comparative study was performed to examine the effect of a silane layer positioned in between a bonding agent and a steel surface. Corrosion was observed along the boundary of the bonded CFRP when the scheduled environmental exposure period was completed. The strength degradation of the specimens was noticed, while the presence of silane partially mitigated interfacial damage. Al-Shawaf (2011) developed a two-dimensional finite element model to predict the behavior of CFRP-steel interface at various temperatures from -40°C to 60°C . Thermal properties of individual materials such as steel, CFRP, and adhesive were taken into account, including their failure criteria. Strain development and failure modes were elaborated. Nguyen et al. (2011) tested double-lap CFRP-steel joints exposed to elevated temperatures ranging from 20°C to 60°C . The glass transition temperature of the adhesive used was 42°C . Thermal stresses altered the failure mode of the joints from adherend failure to debonding failure, and increased the effective bond length of the CFRP. An analytical model was employed to estimate the strength degradation of the joints caused by thermal load. Nguyen et al. (2012) used a similar test protocol to examine the behavior of CFRP-steel joints in a salted water environment and reported the strength and stiffness of the joints decreased. One of a few unexplored areas in CFRP-steel interface behavior is galvanic-current-induced distress and corresponding consequences. This paper discusses an experimental program concerning the performance of CFRP-steel interface subjected to galvanic current that can induce electrochemical reactions for an accelerated corrosion environment. Of interest are the formation of hydrated ferric oxide and the progression of corrosion as well as mechanical responses in terms of interfacial capacity and deformation. A theoretical framework is proposed to examine the deterioration of the interface with the aid of probabilistically inferred fracture energy.

2. RESEARCH SIGNIFICANCE

The behavior of CFRP-steel interface is an intriguing subject in addition to its physical significance in structural strengthening. A number of research projects have been conducted in various technical aspects, including stress distribution issues and failure mechanisms as discussed earlier. It is, however, recognized that insufficient efforts have been made on evaluating the long-term sustainability of interface exposed to aggressive service environments, particularly galvanic-current-induced deterioration, which restricts the knowledge of current state-of-the-art in the rehabilitation community. Such problems can occur when CFRP-strengthened structures consisting of numerous conductive steel elements are exposed to an electrolyte (e.g., leaking of water with deicing salts in a bridge superstructure). In this research, the degradation of interfacial performance due to galvanic current is characterized from experimental and theoretical perspectives. Electrochemical reactions are examined and corrosion-dependent interfacial capacity is explained along with the phase transition of fracture energy.

3. EXPERIMENTAL PROGRAM

3.1 Specimen Details

Double-lap interface test coupons were prepared with two steel strips (100-mm long by 37-mm wide by 3-mm thick per strip) to be bonded with one layer of CFRP sheet (100-mm long by 37-mm wide by 0.165-mm thick per sheet) on each side, as shown in Figure I.1(a). Surface grinding was performed to enhance adhesion between the CFRP and steel [Figure I.1(b)]. A resin-hardener-mixed epoxy adhesive was employed to bond the sheet to the steel substrate. Table I.1 summarizes the mechanical properties (nominal) of these constituents. After evenly pasting the adhesive along the strips, precut CFRP sheets were positioned and softly pressed to squeeze out epoxy residues. In compliance with the manufacturer’s recommendation, the bonded specimens were cured for a minimum of one week at room temperature and their mass was measured. Seven test categories were planned to evaluate the effect of galvanic current on the performance of the CFRP-steel interface, as listed in Table I.2. The electrochemical-processing time varied from 0 hours to 72 hours and five specimens were used per category, including 35 specimens total.

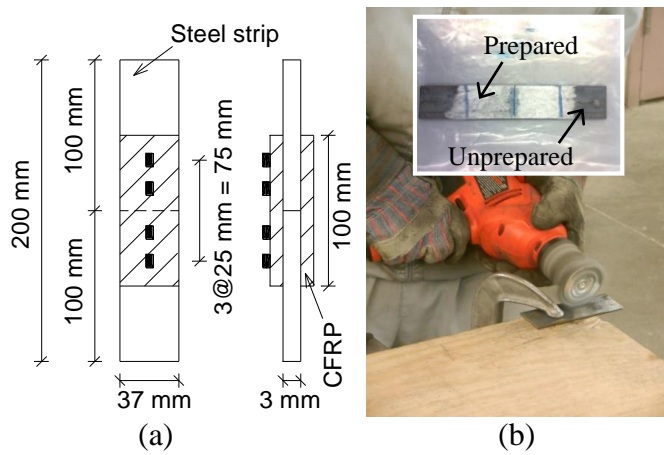


Figure I.1 Specimen details: (a) dimension; (b) surface preparation

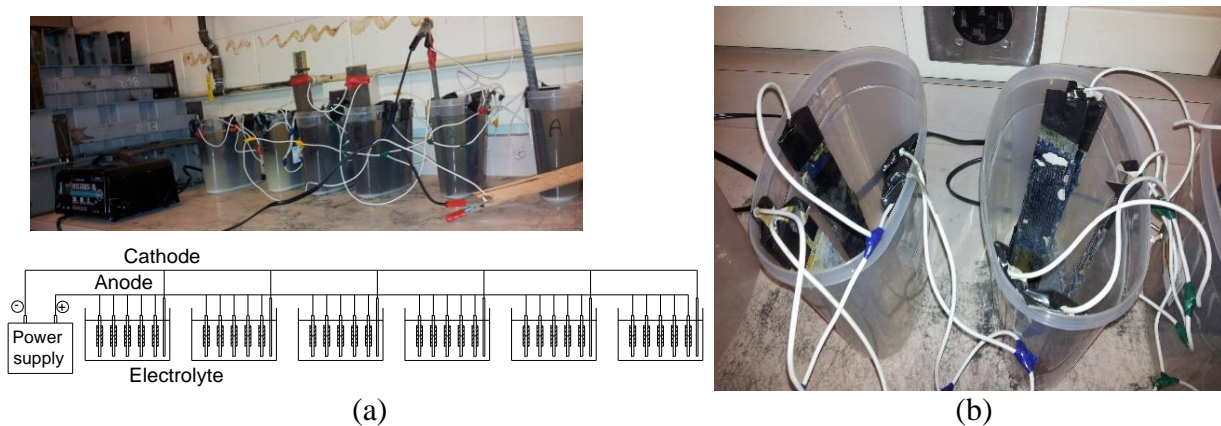


Figure I.2 Galvanic current generating protocol for electrochemical reactions: (a) schematic; (b) close-up view of anodes

Table I.1 Mechanical properties

	Tensile strength (MPa)	Elastic modulus (GPa)	Failure strain (%)
Steel ^a	413	200	0.2
CFRP ^b	3800	227	1.67
Epoxy adhesive	54	3	3.5

^a: yield properties

^b: areal weight = 300 g/m²; coefficient of thermal expansion = $-0.38 \times 10^{-6}/^{\circ}\text{C}$; electrical resistivity = $1.6 \times 10^3 \Omega \text{ cm}$

3.2 Generating Galvanic Current

Galvanic corrosion cells were fabricated with plastic containers, anodes, cathodes, and electrolytes, as shown in Figure I.2. The cured strips served as anodes where oxidation would take place, while additional metallic strips worked as cathodes experiencing reduction; in other words, the anode produced electrons ($\text{Fe} \rightarrow \text{Fe}^{2+} + 2\text{e}^{-}$) that were consumed by the cathode ($1/2\text{O}_2 + \text{H}_2\text{O} + 2\text{e}^{-} \rightarrow 2\text{OH}^{-}$). These two corrosion components were connected by conductive wires to facilitate electrochemical reactions, including an external direct current (DC) power supply (2A). A 3.5% sodium chloride solution was used as the electrolyte conducting a current and transferring the ions for hydrated ferric oxide at room temperature (the temperature in the galvanic cell was not measured). The electrode potential and current of each specimen were measured. It is worth noting that the maximum galvanic current exposure time of 72 hours was determined based on a preliminary test that resulted in a considerable amount of corrosion in the steel strips, whose corrosion rates converged (to be discussed). When the predetermined electrochemical processing time was achieved (Table I.2), all the specimens were retrieved and cleaned as guided by ASTM G1-03 (ASTM 2011).

Table I.2 Summary of test results

Test category	Galvanic current exposure time (hr)	Test data					
		Surface area (cm ²)		Mass loss (kg)		Interfacial capacity (kN)	
		Each	Stdev	Each	Stdev	Each	Stdev
C0	0	173	0.0	0	0.0	28.8	4.2
C12	12	168	3.1	2.5	3.4	23.2	2.5
C24	24	164	3.8	5.7	6.8	21.3	4.5
C36	36	164	3.5	8.7	8.1	22.6	2.8
C48	48	166	6.3	13.2	6.7	20.6	3.5
C60	60	159	1.2	17.7	13.0	15.9	2.8
C72	72	140	15.3	34.0	20.8	6.4	2.9

Stdev = standard deviation

3.3 Post-corrosion Test

3.3.1 Physical Properties

The surface area and mass of the electrochemically processed test specimens were measured using a pair of calipers and a scale, respectively. The extent of corrosion was estimated by Faraday's law (Ahmad 2006):

$$C_r = C \frac{Mi_{corr}}{n\rho} \quad (I.1)$$

where C_r is the corrosion rate in mm/year; C is a conversion constant (0.00327 for mm/year); M is the atomic weight in g/mol (55.9 g/mol for steel); i_{corr} is the corrosion current density in $\mu\text{A}/\text{cm}^2$; n is the number of electrons ($n = 2$ for Fe^{2+}); and ρ is the density of the steel ($7.85 \text{ g}/\text{cm}^3$).

3.3.2 Mechanical Loading for Residual Capacity

The interface test specimens were monotonically loaded at a rate of 0.5 mm/min using a 90 kN capacity universal testing machine, as shown in Figure I.3. To monitor the initiation and progression of CFRP debonding along the interface, strain gages were bonded at a typical spacing of 25 mm on center [Figure I.1(a)]. The applied load and corresponding displacement were recorded by a load cell and a loading-head stroke, respectively.



Figure I.3 Post-corrosion monotonic tension test

4. RESULTS AND DISCUSSION

4.1 Formation of Hydrated Ferric Oxide

Figure I.4 compares the state of the specimens before and after the galvanic current processing. Hydrated ferric oxide, $\text{Fe}(\text{OH})_2$, formed along the steel strips (brown rust) because of the coupled reactions between the anodes and cathode in conjunction with passing of the iron ions into the electrolyte. The corroded steel surface was heterogeneous, and the edge of the specimens tended to exhibit more corrosion damage than other regions. Such an irreversible process resulted in a physical change in the specimens, as shown in Figure I.5. The surface area of the steel strips gradually decreased with an increase in electrochemical reaction time [Figure I.5(a)]. The surface area of the corroded specimens normalized by the average area of the 0-hour counterparts indicated that 18.7% of the surface area was lost at 72 hours, while the normalized area was reasonably maintained up to 60 hours. These observations can be explained by the fact that the progression of corrosion damage was relatively uniform over the steel strips, whereas localized corrosion was accelerated near the corner of the specimens as the effect of galvanic current augmented. The relationship between the variation of mass and corrosion time is available in Figure I.5(b). Although some scatter was noticed in all cases, it is apparent that the electrochemical reaction entailed a noticeable decrease in specimen mass up to 19.0% of the initial mass, on average, at 72 hours.

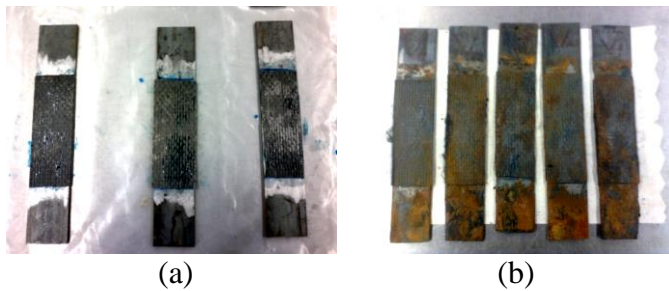


Figure I.4 Effect of galvanic current: (a) control; (b) specimens exposed to 36 hours

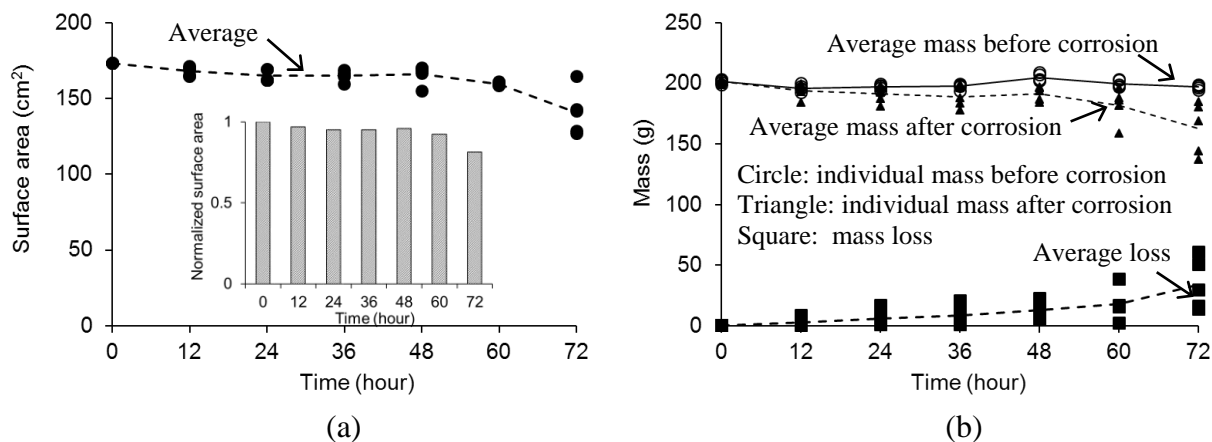


Figure I.5 Variation of physical properties with time: (a) surface area; (b) mass loss

4.2 Corrosion Rate

Figure I.6 shows the rate of corrosion (Eq. I.1) depending upon reaction hours. A propensity for an exponentially decreasing rate was observed, while the variation beyond 48 hours was not significant (i.e., the average corrosion rate from 48 hours to 72 hours was 0.05 mm/yr). This fact implies that electrochemical reaction was active when corrosion initiated; however, it tended to dwindle with an increase in time. Similar observations were reported by others (Yalcyn and Ergun 1996; Liu and Weyers 1998). Vu and Stewart (2000) noted that the diffusion of iron ions can be affected by the rust formed over a steel surface so that the progression of corrosion slows down as time increases due to the accumulated rust amount. Figure I.6 also compares the corrosivity of steel members exposed to various exposure conditions specified by ISO-9224 (ISO 2012): High (C4), Very high (C5), and Extreme (CX). The average experimental corrosion rate of 0.12 mm/yr was positioned between the C5 and CX categories, which is reasonable because the electrochemical reaction with galvanic current imposed on the CFRP-steel interface resulted in an accelerated corrosion environment that could represent aggressive service conditions.

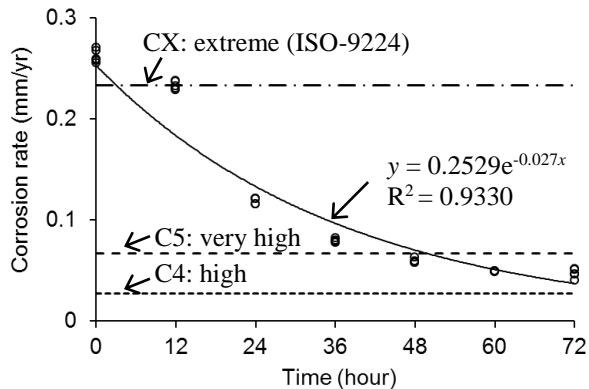


Figure I.6 Corrosion propagation with time

4.3 Interfacial Capacity

Figure I.7 reveals the interfacial capacity of the individual specimens. The initiation of corrosion damage within the CFRP-steel interface was apparent due to the galvanic current flowed, entailing the 19.5% average capacity drop between the reaction time of 0 and 12 hours. With an increase in corrosion-processing time from 12 hours to 24 hours, the percentage of the capacity drop was reduced down to 8.4%. In between 24 hours and 48 hours, the interfacial capacity remained virtually unchanged. A significant capacity reduction was noticed beyond 48 hours, including an average drop of 77.7% for the specimens exposed to 72 hours in comparison with the strength of the un-corroded specimens (0 hours). Irrespective of the extent of electrochemical reactions, all interface specimens failed by CFRP-debonding when mechanically loaded (Figure I.8). Disintegration of the CFRP composite itself was not observed in the corroded specimens from a macro-scale standpoint. In other words, the galvanic current primarily deteriorated the steel substrate (and the CFRP-steel interface), rather than the CFRP. It is thought that the adhesive layer has impeded galvanic interaction between the steel and the conductive carbon fibers. This finding clarifies that an additional protection layer between the CFRP and steel is not necessary (e.g., glass FRP sheets may be positioned in between the steel substrate and CFRP to

mitigate the occurrence of galvanic corrosion as used in some experimental programs, Mertz and Gillespie 1996; Shaat and Fam 2008), as long as the bonding agent is properly applied along the steel substrate.

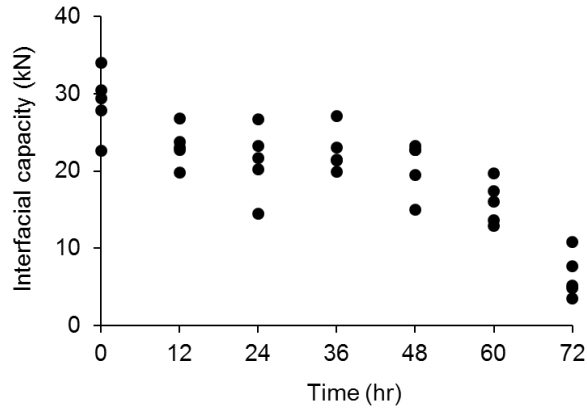


Figure I.7 Interfacial capacity of specimens

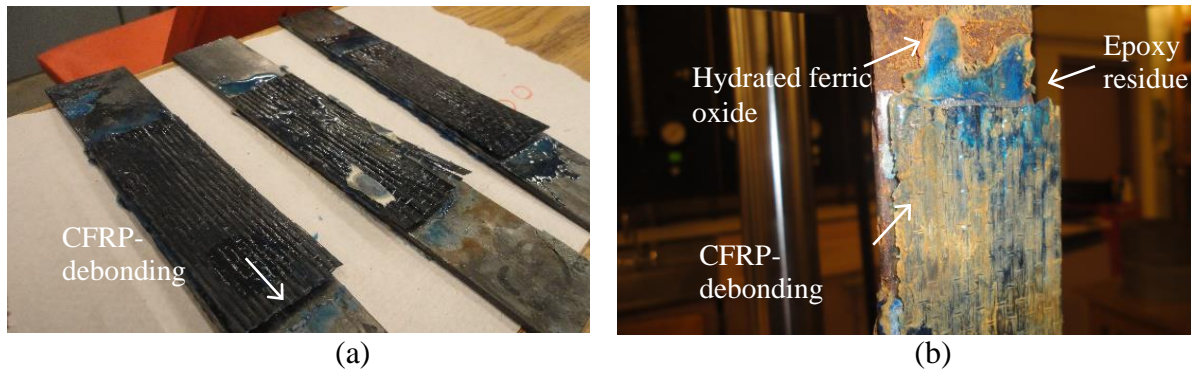


Figure I.8 Failure mode: (a) without galvanic current processing (0 hours); (b) with galvanic current processing (24 hours)

4.4 Displacement and Strain Response

The load and displacement behavior of selected interfacial specimens is depicted in Figure I.9. The displacement of the specimens increased linearly with the load until abrupt failure took place. As discussed in the previous sections, some scatter was noticed in capacity and stiffness because of uneven corrosion progression along the interface. Although all the responses were intrinsically brittle, some specimens in the 72-hour exposure category [Figure I.9(d)] demonstrated gradual load-softening after their peak loads were achieved. Such a fact points out that the bonded steel surface was partially damaged by the formation of the hydrated ferric oxide; hence, the mechanical failure of the interface occurred in a progressive manner. Figure I.10 describes the variation of the stiffness depending upon the level of electrochemical processing time. It was unlikely to characterize the effect of galvanic current on the response of the interfacial stiffness; nonetheless, the average stiffness of all the specimens (10.2 kN/mm) could be a reference value for the CFRP-steel interface exposed to a corrosive environment. Figure I.11 provides the strain development of the CFRP-steel interface with respect to the

applied load. A general trend found was that strain gages bonded near the middle of the specimen (Gages 2 and 3) showed early CFRP-debonding, which was indicated by a bifurcation from the ascending linear load-strain branch. This is because the gap between the two steel strips [Figure I.1(a)] caused stress singularity. Such premature local debonding may be observed in full-scale steel girders strengthened with CFRP sheets when geometric discontinuity occurs (e.g., fatigue cracking).

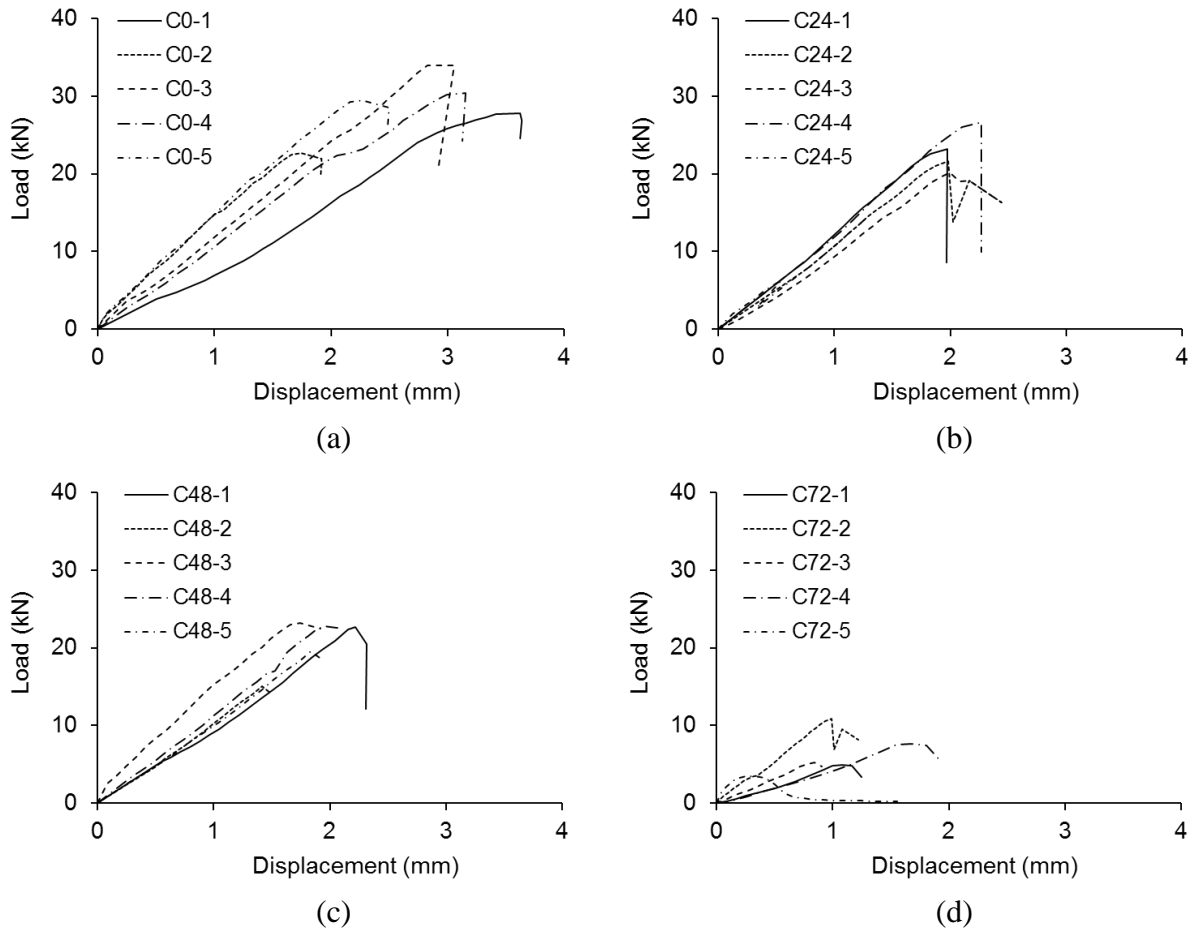


Figure I.9 Load-displacement behavior: (a) 0 hours; (b) 24 hours; (c) 48 hours; (d) 72 hours

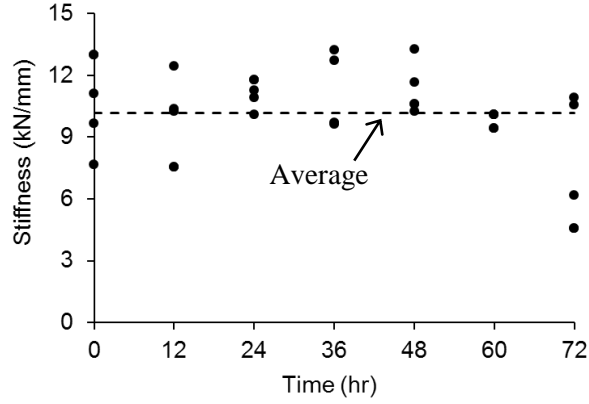


Figure I.10 Stiffness of the specimens

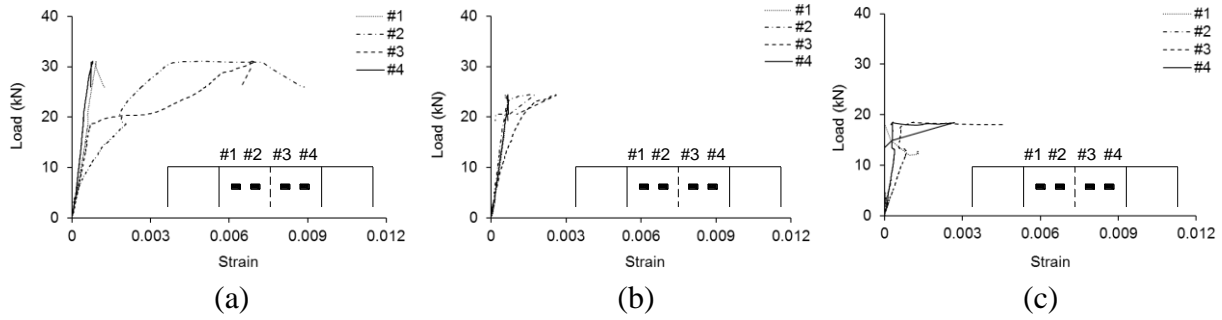


Figure I.11 Load-strain behavior: (a) 0 hours; (b) 24 hours; (c) 48 hours

4.5 Bond-slip Behavior

Figure I.12 summarizes the bond-slip behavior of the CFRP-steel interface experiencing various levels of the galvanic current flow. Equations I.2 and I.3 were employed to calculate the interfacial stress and associated slip of the CFRP, respectively:

$$\tau = E_F t_F \frac{\Delta \varepsilon(x)}{\Delta x} \quad (\text{I.2})$$

$$s = \int_{x_1}^{x_2} \varepsilon(x) dx \quad (\text{I.3})$$

where τ is the average interfacial stress between two arbitrary spatial locations (x_2 and x_1) exhibiting a strain gradient $\Delta \varepsilon(x)$; Δx is the distance between the two locations; E_F and t_F are the elastic modulus and thickness of the CFRP, respectively; s is the slip of the CFRP over the steel substrate. For the un-corroded 0-hour interface [Figure I.12(a)], the middle of the specimen (Location 2) where a geometric discontinuity existed showed multiple ascending and descending stress-slip responses; on the other hand, the interfacial stresses at locations 1 and 3 (outside the discontinuity) continuously developed up to their peak along with an increase in slip. These

observations illustrate that i) the propagation of local CFRP-debonding was gradational in the vicinity of the discontinuity (possibly accompanying complex interaction between the bonded and partially-debonded regions), and ii) the behavior of the CFRP-steel interface outside the stress singularity zone was preserved until the gradational debonding progressed. The electrochemical reaction induced by the galvanic current altered the stress-slip behavior of the interface, as revealed in Figure I.12(b) and (c). The aforementioned stress development pattern was maintained even though the extent was reduced noticeably. Figure I.13 demonstrates the influence of reaction time on the maximum interfacial stresses of the specimens. As mentioned earlier, the stress significantly decreased when electrochemical damage was initiated and was gradually reduced as the galvanic current propagated. The increased stresses at 60 and 72 hours could be explained by the fact that corrosion-induced impurities on the steel substrate augmented frictional resistance in conjunction with CFRP slip, which resulted in an increase in strain gradient (Eq. I.2).

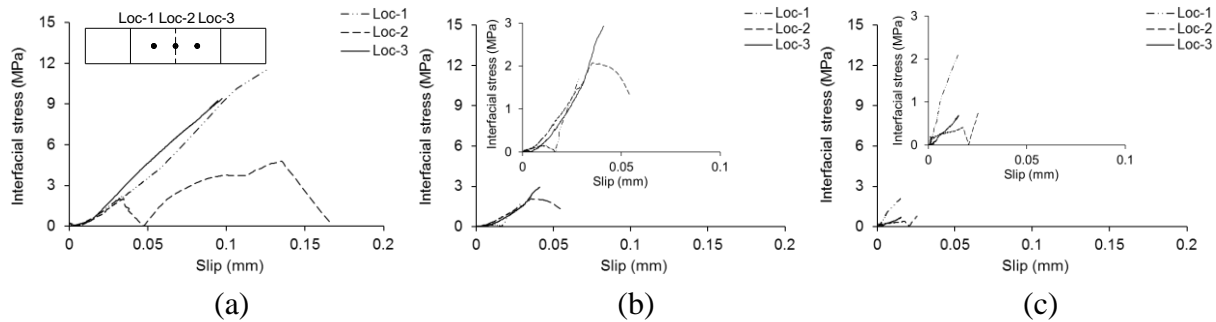


Figure I.12 Interfacial stress-slip behavior: (a) 0 hours; (b) 24 hours; (c) 48 hours

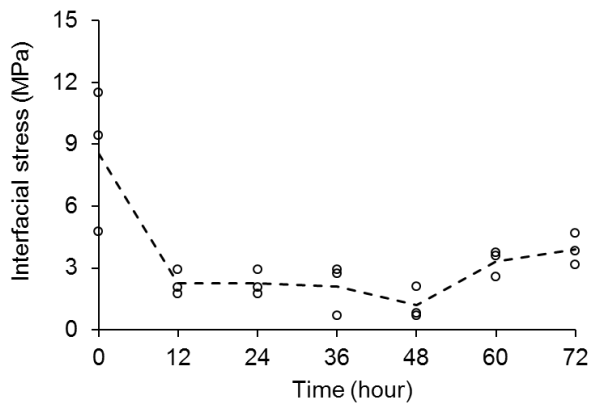


Figure I.13 Comparison of maximum local interfacial stresses

5 MODELING OF INTERFACE DETERIORATION

5.1 Formulation of Theory

Assuming the deterioration of the CFRP-steel interface is a function of galvanic current exposure time, Eq. I.4 may be established:

$$D = \left(\frac{t_i}{t_f} \right)^n \quad (\text{I.4})$$

where D is the level of deterioration varying from 0 (intact) to 1 (complete deterioration); t_i and t_f are the arbitrary exposure time and the time at complete deterioration, respectively; and n is an empirical constant depending upon exposure conditions. To determine the constant n , the logarithm of Eq. I.4 can be taken:

$$n = \frac{\log D}{\log t_i - \log t_f} \quad (\text{I.5})$$

The probability of deterioration (P_{rD}) in terms of an interfacial fracture energy (G_f) distribution may be inferred by Eq. I.6:

$$P_{rD} = 1 - A_{ti} \quad (\text{I.6})$$

where A_{ti} is the overlapped area between the control probability distribution curve of the intact interfacial fracture energy and the conditioned probability curve at time t_i . The parameter t_f is then defined as the time when the overlapped area A_{ti} of the two fracture energy curves becomes approximately zero (the probability distributions of the control and conditioned curves are extended to infinity). Brosens and van Gemert (1999) proposed a simple analytical equation for the interfacial capacity of a substrate (P_u) bonded with a thin plate:

$$P_u = b_p \sqrt{2G_f E_p t_p} \quad (\text{I.7})$$

where b_p is the width of the plate, and E_p and t_p are the elastic modulus and thickness of the plate, respectively. The corrosion-dependent fracture energy of the CFRP-steel interface may be derived from Eq. I.7:

$$G_f(t_i) = \left(\frac{P_u(t_i)}{b_p} \right)^2 \frac{1}{2E_p t_p} \quad (\text{I.8})$$

where $G_f(t_i)$ is the fracture energy of the CFRP-steel interface subjected to galvanic current exposure time t_i and $P_u(t_i)$ is the corresponding capacity of the interface. Knowing the constants n and t_f , the rate of interface deterioration with respect to galvanic current exposure time t_i is obtained by:

$$\frac{dD}{dt} = \frac{n}{t_f^n} t_i^{n-1} \quad (\text{I.9})$$

Equation I.9 is, in principle, equivalent to the progression of corrosion damage in the CFRP-steel interface.

5.2 Implementation

5.2.1 Fracture Energy

Figure I.14(a) summarizes the variation of the interfacial fracture energy with respect to exposure time (Eq. I.8). Three performance stages linked with corrosion damage were noticed: initiation, steady-state progression, and decaying. The interfacial fracture energy within the first stage was rapidly reduced from 8.3 N/mm to 5.3 N/mm at 0 hours and 12 hours (0.25 N/mm per hour), on average; on the other hand, the average fracture energy drop in the steady-state progression zone was 0.03 N/mm per hour from 12 hours to 48 hours. Within an exposure period between 60 and 72 hours, the degradation of the interfacial fracture energy was accelerated to 0.17 N/mm per hour. From a practical perspective, the initiation and steady-state progression stages can typically occur during the service life of a CFRP-strengthened steel member; however, the decaying stage may be observed at discrete locations where corrosion damage is concentrated, rather than along the entire interface. The coefficient of variation (COV) of the fracture energy was almost constant up to 60 hours with an average value of 0.30, as shown in Figure I.14(b), whereas the COV of 72 hours was much higher than others, possibly because of the unstable interfacial bond associated with substantial corrosion on the steel substrate (i.e., a mix of bonded and unbonded regions as previously explained).

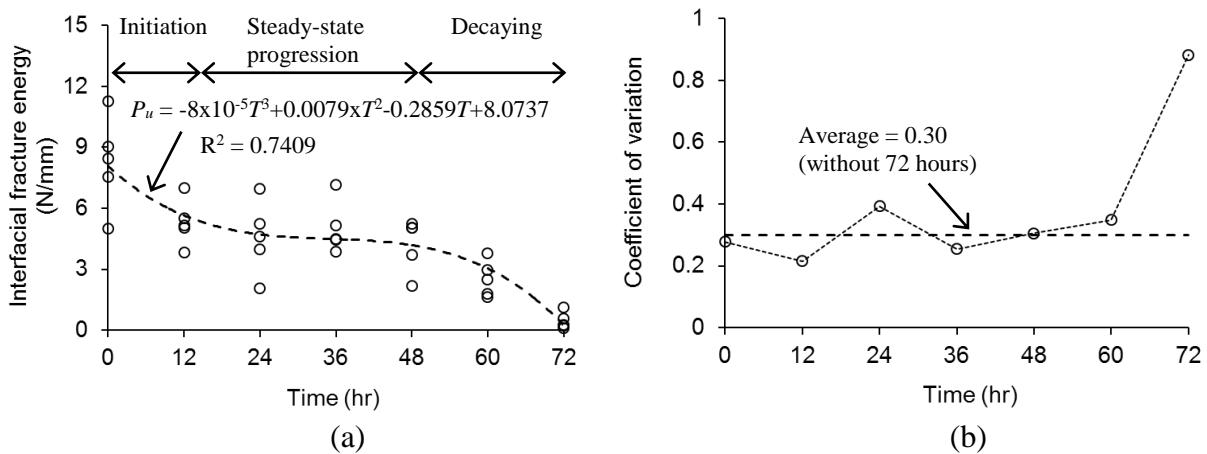


Figure I.14 Interfacial fracture energy: (a) variation with exposure time; (b) coefficient of variation

5.2.2 Probabilistic Response

All the semi-experimentally determined interfacial fracture energy values were sorted and used for determining the type of a probability distribution. Equation I.10 shows a typical normality test method to calculate an inverse standard normal distribution:

$$z_i = \Phi^{-1}\left(\frac{G_{fi} - a}{k + 1 - 2a}\right) \quad (\text{I.10})$$

where Φ is the standard normal quantile function, G_{fi} is the sorted interfacial fracture energy, k is the total specimen number, and a is a constant ($a = 0.375$ and 0.5 for $k \leq 10$ and $k > 10$, respectively). The relationship between the inverse standard normal distribution and the interfacial fracture energy is provided in Figure I.15. Significant linearity was observed with a coefficient of determination of $R^2 = 0.9659$. It is, therefore, concluded that the corrosion-dependent fracture energy of the CFRP-steel interface had a normal probability distribution. Figure I.16(a) reveals the transition of the inferred probability distributions, depending upon galvanic current exposure time, in accordance with the best-fit fracture energy formula and the average COV of 0.30 as shown in Figure I.14. The phase transition of the interfacial fracture energy was obvious with an increase in exposure hour (i.e., the most probable fracture energy became pronounced). The distribution of 72-hour exposure was not available because the interface was predicted to fail (i.e., complete deterioration, $D = 1$ and $n_f = 72$ hours). The probability of interface deterioration (Eq. I.6) is available in Figure I.16(b). A deterioration probability of 0.42 was noticed at 12 hours, which implies that the CFRP-steel interface was susceptible to damage when corrosion initiated, while the progression of the deterioration probability was relatively consistent until 72 hours was reached.

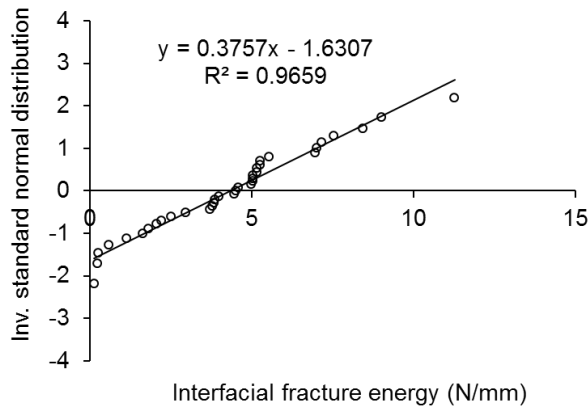


Figure I.15 Normality check for test specimens

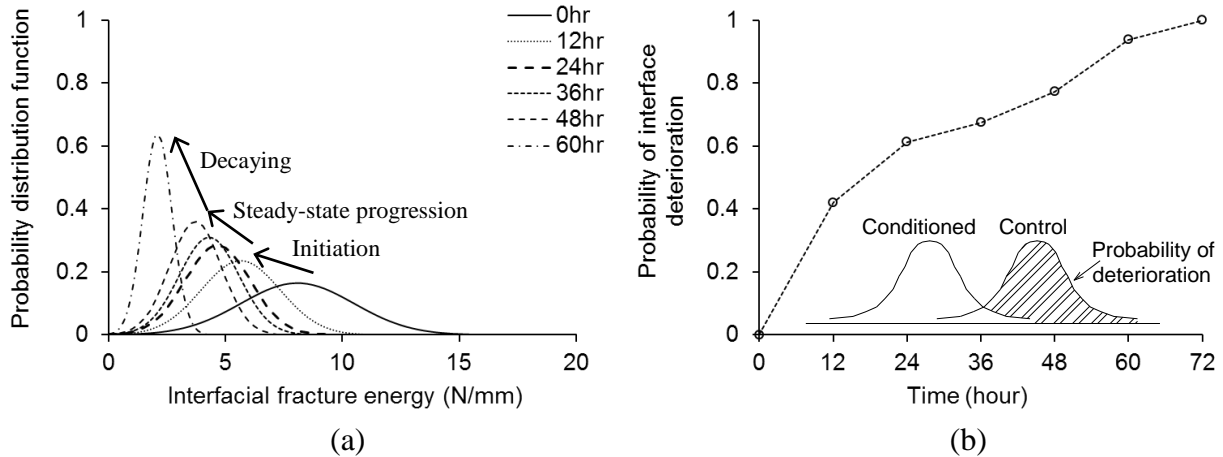


Figure I.16 Predicted response of interfacial fracture energy: (a) effect of galvanic current exposure time; (b) probability of interface deterioration

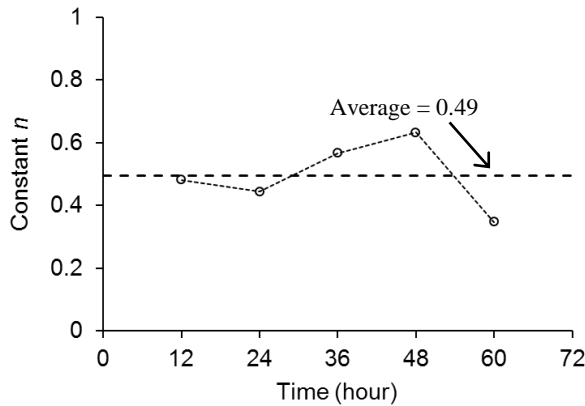


Figure I.17 Determination of deterioration constant

5.2.3 Interface Deterioration

The empirical constant n of Eq. I.5 was acquired by Figure I.17 (individual n values for 0 hours and 72 hours were not obtainable by definition), including an average value of $n = 0.49$. All the empirical constants determined previously were substituted into Eq. I.4, and the level of interface deterioration was predicted, as shown in Figure I.18(a). It was estimated that deterioration levels of 0.25 and 0.5 could take place at 7% and 25% of the failure time ($t_i/t_f = 0.7$ and 0.25), respectively. Figure I.18(b) illustrates the rate of interface deterioration. A rapid increase in deterioration rate was observed at the beginning of CFRP-strengthening, followed by an exponentially decreasing trend with time. Such a predicted deterioration rate was aligned with the corrosion rate presented in Figure I.6, and theoretically corroborates the aforementioned assertion concerning the interrupted diffusion process of iron ions as the amount of surface rust augmented.

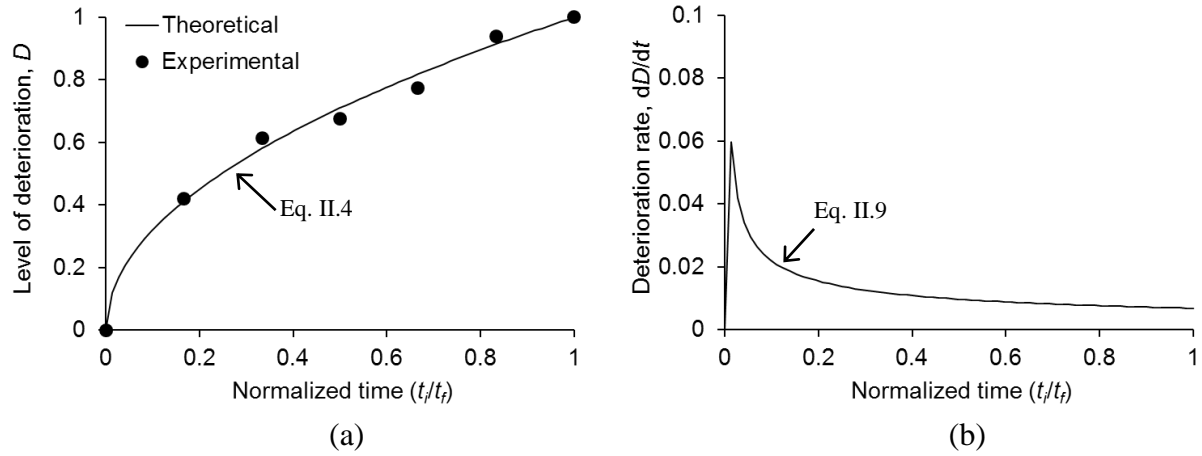


Figure I.18 Deterioration of CFRP-steel interface: (a) progression of deterioration level; (b) development of deterioration rate

6. SUMMARY AND CONCLUSIONS

This paper has discussed the effect of galvanic current on the behavior of the CFRP-steel interface, including changes in physical properties and mechanical characteristics. An electrochemical reaction protocol was employed to provide an accelerated corrosion environment, which degraded the performance of the interface. The corrosion-dependent response of the interface was experimentally characterized and a modeling approach was proposed to predict the propagation of interface deterioration. Further research may be required to correlate the accelerated test results with the in-situ performance of CFRP-strengthened steel structures exposed to aggressive service environments. The following conclusions are drawn:

- The coupled reactions between the anodes and cathodes resulted in hydrated ferric oxide along the CFRP-steel interface, while the edge of the specimens attracted more corrosion damage in conjunction with a noticeable loss in their surface area and mass.
- The variation of the corrosion rate clarified that the electrochemical reaction in the CFRP-steel interface decayed exponentially as a galvanic current exposure time increased. The diffusion process of iron ions appeared to slow down because of the accumulated rust along the test specimens.
- The load-carrying capacity of the interface was influenced by the rate of corrosion in such a sense that the capacity drop when corrosion damage initiated was 232% greater, on average, than the drop within a steady-state corrosion progression period. Some load-softening was noticed due to the formation of hydrated ferric oxide that partially degraded the steel surface (a mix of bonded and unbonded CFRP regions). A protection layer between the steel substrate and the CFRP for the sake of mitigating galvanic interaction was found to be unnecessary.
- CFRP-debonding was the predominant failure mode for all the test specimens, regardless of the extent of galvanic current exposure. Stress singularity caused the initiation of debonding, entailing a bifurcation of strain development in the ascending branch of the load-strain behavior. The stress-slip response of the interface was also affected by the electrochemical reaction.
- The probability distribution of the corrosion-dependent interfacial fracture energy was found to be normal, with an average coefficient of variation of 0.30. The probability-based theoretical framework predicted the degree of interface deterioration subjected to an aggressive service environment, in particular, corrosive circumstances.

7. REFERENCES

- ASTM. 2011. Standard practice for preparing, cleaning, and evaluating corrosion test specimens, American Society for Testing and Materials, West Conshohocken, PA.
- Ahmad, Z. 2006. Principles of corrosion engineering and corrosion control, Butterworth Heinemann, Oxford, UK.
- Al-Shawaf, A. "Modelling wet lay-up CFRP-steel failures at extreme temperatures using stress-based approach," *International Journal of Adhesion and Adhesives*, 31, 416-428.
- Brosens, K., and van Gemert, D. 1999. Anchorage design for externally bonded carbon fiber reinforced polymer laminates, Proceedings of the 4th International Symposium on Fiber Reinforced Polymer Reinforcement for Concrete Structures, 635-645.
- Cadei, J.M., Stratford, T.J., Hollaway, L.C., and Duckett, W.G. 2004. "Strengthening metallic structures using externally bonded fibre-reinforced polymers," *CIRIA*, Publication C595, London, UK.
- Egilmez, O.O., and Yormaz, D. 2011. "Cyclic testing of steel I-beams reinforced with GFRP," *Steel and Composite Structures*, 11(2), 93-114.
- FHWA. 2014. National bridge inventory: bridges by structure type, Federal Highway Administration, Washington, D.C.
- Gholami, M., Sam, A.R.M., Yatim, J.M., and Tahir, M.M. 2013. "A review on steel/CFRP strengthening systems focusing environmental performance," *Construction and Building Materials*, 47, 301-310.
- Hollaway, L.C., and Cadei, J. 2002. "Progress in the technique of upgrading metallic structures with advanced polymer composites," *Progress in Structural Engineering and Materials*, 4, 131-148.
- ISO. 2012. Corrosion of metals and alloys (ISO 9224), International Organization for Standardization, Geneva, Switzerland.
- Liu, T., and Weyers, R.W. 1998. Modeling the dynamic corrosion process in chloride contaminated concrete structures, 28(3), 365-379.
- Mertz, D.R., and Gillespie, J.W. 1996. Rehabilitation of steel bridge girders through application of advanced composite material, NCHRP Report No. 93-ID11, Transportation Research Board, Washington, D.C.
- Nguyen, T.C., Bai, Y, Zhao, X-L., and Al-Mahaidi, R. 2011. "Mechanical characterization of steel/CFRP double strap joints," *Composite Structures*, 93, 1604-1612.

Nguyen, T.C., Bai, Y, Zhao, X-L., and Al-Mahaidi, R. 2012. "Durability of steel/CFRP double strap joints exposed to sea water, cyclic temperature and humidity," *Composite Structures*, 94, 1834-1845.

Shaat, A., and Fam, A. "Repair of cracked steel girders connected to concrete slabs using carbon-fiber-reinforced polymer sheets," *Journal of Composites for Construction*, 12(6), 650-659.

Shokrieh, M., and Bayat, A. 2007. "Effects of ultraviolet radiation on mechanical properties of glass/polyester composites," *Journal of Composite Materials*, 41, 2443-2455.

Smith, S.T., and Teng, J.G. 2001. "Interfacial stresses in plated beams," *Engineering Structures*, 23(7), 857-871.

Tao, Z., Han, L.-H., and Zhung, J.-P. 2007. "Axial loading behavior of CFRP strengthened concrete-filled steel tubular stub columns," *Advances in Structural Engineering*, 10(1), 37-46.

Tavakkolizadeh, M., and Saadatmanesh, H. 2001. "Galvanic corrosion of carbon and steel in aggressive environments," *Journal of Composites for Construction*, 5(3), 200-210.

Teng, J.G., Yu, T., and Fernando, D. 2012. "Strengthening of steel structures with fiber-reinforced polymer composites," *Journal of Constructional Steel Research*, 78, 131-143.

Vu, K.A.T., and Stewart, M.G. 2000. "Structural reliability of concrete bridges including improved chloride-induced corrosion models," *Structural Safety*, 22, 313-333.

Yalcyn, H. and Ergun, M. 1996. "The prediction of corrosion rates of reinforcing steels in concrete," *Cement and Concrete Research*, 26(10), 1593-1599.

Zhao, X.L. and Zhang, L. 2007. "State-of-the-art review on FRP strengthened steel structures," *Engineering Structures*, 29(8), 1808-1823.

Part II: Electrochemical Reaction for Steel Beams Strengthened with CFRP Sheets

8. INTRODUCTION

The deterioration of a steel girder bridge (e.g., fatigue-induced crack) is a critical consideration because it will influence flexural behavior, including load-carrying capacity, which is of interest from ultimate limit state perspectives. Stress concentrations at geometric discontinuities can accelerate damage propagation; hence, timely rehabilitation is necessary to save long-term repair costs. Carbon fiber reinforced polymer (CFRP) is a promising material for strengthening damaged steel members due to the following benefits: favorable strength-to-weight ratio, resistance to corrosion and fatigue, rapid execution in practice, and reduced maintenance expenses (Hollaway and Cadei 2002). The primary focus of existing research related to CFRP-strengthening for steel structures is on mechanical responses such as flexural capacity and failure modes (Teng et al. 2012). There is a dearth of understanding the behavior of strengthened steel beams subjected to environmental distress (Gholami et al. 2013; Zhao et al. 2014). The durability of interfacial bond between the CFRP and steel substrate has recently attracted the research community. Grant et al. (2009) examined the strength of adhesively bonded steel joints in temperature-induced loading from -40°C to 90°C . A comparative study was performed to evaluate the failure criterion of such a joint at room and variable temperatures. Experimental results revealed that geometric configurations of the adhesive affected interfacial strength, and the failure criterion established could be used regardless of temperature exposure within the investigation range. Doyle and Pethrick (2009) reported the behavior of epoxy-bonded metallic interface in aggressive environmental conditions, including de-ionized water, aqueous urea solution, and salt water. Plasticization and substrate-corrosion changed interfacial capacity. Dawood and Rizkalla (2010) carried out an experimental program examining the capacity of CFRP-steel interface exposed to an aggressive environment. Degradation of bond strength was monitored with time, and failure modes were observed. Test data were employed to assess existing design guidelines.

Corrosion is induced by an electrochemical reaction mechanism and is considered to be one of the most critical attributes degrading the performance of constructed steel structures (Albrecht and Hall 2003; Rahgozar 2009; O'Connor et al. 2013). CFRP-strengthened steel members are also vulnerable to corrosion damage. The following hypothesis may be proposed: surface rust formed by the oxidation of iron ions reacting with hydroxide affects the behavior of CFRP sheets bonded to a steel substrate. This important technical aspect, however, is not well documented in the literature. The present research addresses the effect of electrochemical corrosion on the performance of steel beams strengthened with CFRP sheets. An experimental program has been conducted with an electrochemical protocol to characterize corrosion damage and corresponding consequences in terms of structural and chemical responses of the strengthening system. All test findings are integrated to develop design recommendations for promoting CFRP-strengthening technologies.

9. EXPERIMENTAL PROGRAM

9.1 Materials

A992 structural steel has a nominal yield strength of 345 MPa and an elastic modulus of 200 GPa, along with an ultimate strength of 450 MPa (ASTM 2011). The tensile strength and modulus of the unidirectional wet-layup CFRP sheets used (CF-130) are 3,800 MPa and 227 GPa, respectively, according to the manufacturer's datasheet based on an equivalent thickness of 0.165 mm. A two-part epoxy adhesive (MBrace Saturant) was employed to bond the CFRP to a steel substrate. The epoxy is a low viscous product (1600 cps at 20°C) and has a tensile strength of 54 MPa with a modulus of 3 GPa.

9.2 Specimen Preparation

A total of 22 beams were prepared, including one un-strengthened, three un-corroded, and 18 corroded beams. W100×19 steel beams were precut to a length of 1,000 mm. A notch of 30 mm at midspan was created using a blade saw to simulate structural damage (e.g., fatigue cracking), as shown in Figure II.1(a). Such a damage configuration is often used when examining the flexural behavior of CFRP-strengthened steel beams (Nozaka et al. 2005; Shaat and Fam 2008; Nakamura et al. 2009). Another purpose of the notch was to initiate CFRP-debonding at midspan for observing a consistent failure pattern, regardless of test configurations. Before bonding the CFRP sheet, the steel substrate was ground using an electric steel brush to enhance bond between the steel and the CFRP and was cleansed with an air compressor. Other surface preparation methods, such as grit-blasting, are also available, while according to the authors' previous experience, the performance of adhesively bonded CFRP was virtually independent of preparation techniques as long as the surface is sufficiently roughened and the robust chemical bonding of polymeric adhesives controls the interfacial behavior. The mixed epoxy was pasted on the prepared steel surface and one layer of CFRP sheet (100 mm wide×0.165 mm thick×700 mm long) was impregnated. To squeeze out excessive epoxy residues, the CFRP surface was softly rubbed with a spatula (an adhesive thickness of about 1 mm was achieved along the bond-line). All the CFRP-bonded beams were cured for seven days at room temperature prior to commencing an electrochemical process.

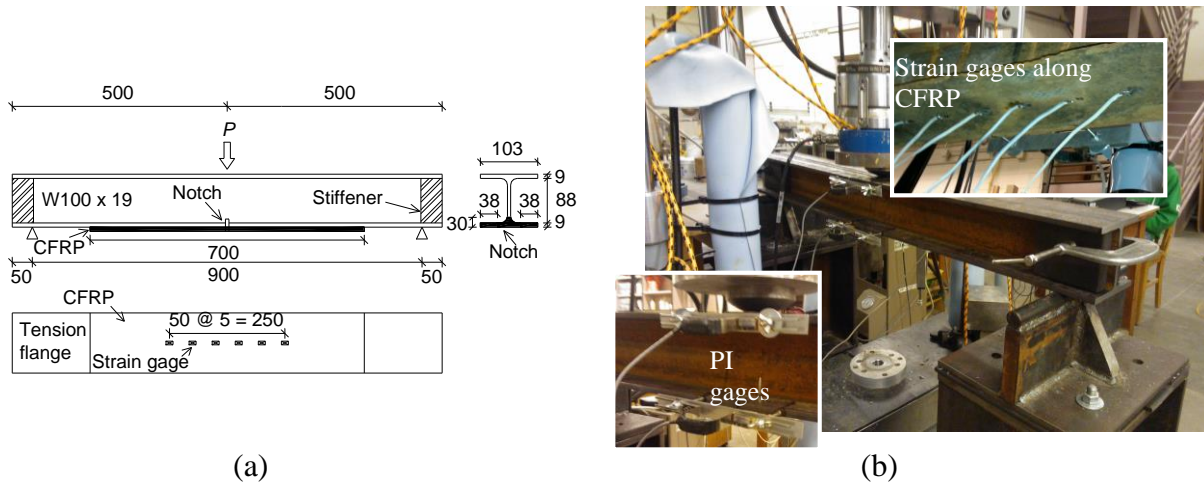


Figure II.1 Beam details: (a) dimensions (unit in mm); (b) flexural test and instrumentation

9.3 Accelerated Corrosion

An electrochemical reaction cell was exploited for accelerated corrosion testing, as schematically shown in Figure II.2(a). The corrosion cell consisted of an external power supply (2A direct current), anodes (steel beams), a cathode (a metallic strip), an electrolyte (3.5% NaCl solution that is commonly used in accelerated corrosion test programs), and connecting wires between the cathode and anodes. Upon generating electricity, the anode beams lost electrons ($\text{Fe} \rightarrow \text{Fe}^{2+} + 2\text{e}^-$) and the electrolyte expedited oxidation ($4\text{Fe}^{2+} + \text{O}_2 \rightarrow 4\text{Fe}^{3+} + 2\text{O}^{2-}$) associated with a reduction reaction at the cathode ($\text{O}_2 + 2\text{H}_2\text{O} + 4\text{e}^- \rightarrow 4\text{OH}^-$). Brown rust then formed around the steel beams with increasing time [Figure II.2(b)]. During this electrochemical process, the electrical potential and current of the beams were monitored. The CFRP-strengthened beams submerged in the electrolyte were subjected to a simulation period from 12 hours to 72 hours at a typical interval of 12 hours (the electrochemical responses of the beams approached zero at 72 hours, and this was determined from a preliminary test), as listed in Table II.1: three beams were simultaneously exposed to each corrosion environment.

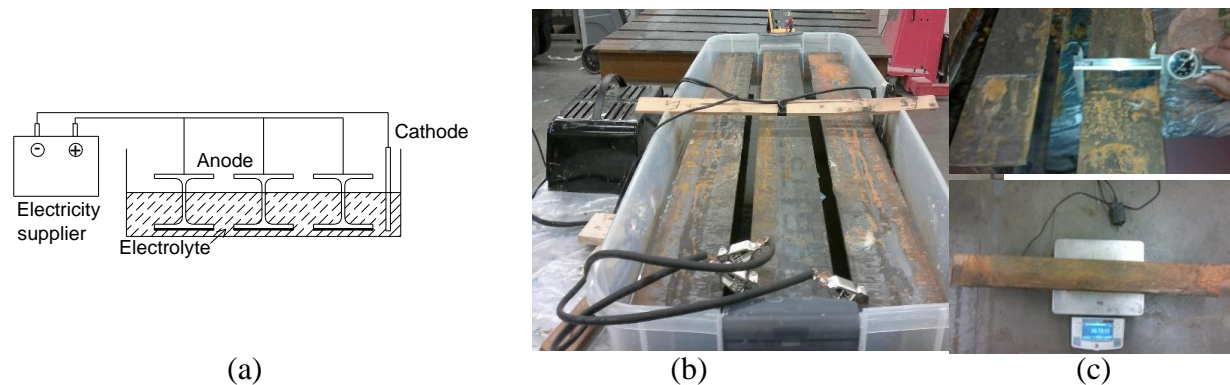


Figure II.2 Electrochemical reaction: (a) schematic; (b) test in progress; (c) measuring surface area and mass loss

Table II.1 Test matrix for CFRP-strengthened beams

Specimen	Exposure time	Surface area (cm ²)		Mass loss (kg)		Ultimate load (kN)	
		Each	Average	Each	Average	Each	Average
B1CR0	0hr	6145	6145	0.00	0.00	62.9	62.9
B2CR0		6145		0.00		63.2	
B3CR0		6145		0.00		62.6	
B1CR12	12hr	6129	6129	0.02	0.03	58.2	58.7
B2CR12		6128		0.04		59.5	
B3CR12		6129		0.03		57.9	
B1CR24	24hr	6097	6096	0.35	0.15	54.2	54.0
B2CR24		6101		0.03		54.4	
B3CR24		6090		0.07		53.5	
B1CR36	36hr	6048	6044	0.27	0.42	49.0	48.3
B2CR36		6043		0.46		47.3	
B3CR36		6041		0.53		48.7	
B1CR48	48hr	6044	6045	0.42	0.46	46.9	46.8
B2CR48		6044		0.54		46.5	
B3CR48		6047		0.41		47.0	
B1CR60	60hr	6033	6034	0.53	0.48	45.6	45.6
B2CR60		6031		0.28		44.8	
B3CR60		6037		0.64		46.4	
B1CR72	72hr	6009	6005	0.46	1.17	43.1	43.0
B2CR72		6008		1.55		42.5	
B3CR72		5997		1.49		43.3	

9.4 Quantification of Corrosion

The mass loss of the specimens is an indicator of estimating the extent of corrosion. After completing the scheduled electrochemical reaction time, the conditioned beams were washed with water to eliminate corrosion residues and completely dried (ASTM G01-03 (ASTM 2011) suggests use of water and reagent grade chemicals for cleaning), then their mass and dimensions (thickness and width all around the specimens) were measured [Figure II.2(c)]. These values were compared with those measured before commencing the electrochemical process (i.e., undamaged state). To estimate the progression of physical damage, the rate of corrosion was calculated by Faraday's law (Ahmad 2006):

$$C_r = C \frac{M_{i_{corr}}}{n\rho} \quad (\text{II.1})$$

where C_r is the corrosion rate in mm/year; C is a conversion constant (0.00327 for mm/year); M is the atomic weight in g/mol (55.9 g/mol for steel); i_{corr} is the corrosion current density in $\mu\text{A}/\text{cm}^2$; n is the number of electrons ($n = 2$ for Fe^{2+}); and ρ is the density of the beam ($7.85 \text{ g}/\text{cm}^3$).

9.5 Efficiency of CFRP-strengthening

Corrosion may result in irreversible damage to the CFRP-steel interface and, as such, the effectiveness of CFRP-strengthening is reduced. By assuming the strengthened beam is regarded as an isolated system, the capacity of the beam can be decomposed into multiple attributes as shown in Eq. II.2:

$$P_{strengthened} = P_{unstrengthened} + P_{CFRP} - P_{loss} \quad (\text{II.2})$$

where $P_{strengthened}$ and $P_{unstrengthened}$ are the capacities of the strengthened and un-strengthened beams, respectively; P_{CFRP} is the contribution of the CFRP; and P_{loss} is the capacity loss induced by corrosion damage. The efficiency of CFRP-strengthening (Ω_{CFRP}) can then be defined as follows:

$$\Omega_{CFRP} = 1 - \frac{P_{loss}}{(P_{0-strengthened} - P_{unstrengthened})} \quad (\text{II.3})$$

where $P_{0-strengthened}$ is the capacity of the strengthened beam without corrosion damage. The larger the efficiency Ω_{CFRP} is, the smaller the degree of irreversibility becomes (i.e., less corrosion damage).

9.6 Flexural Testing and Instrumentation

The control and conditioned beams were simply supported with a span length of 900 mm and monotonically loaded at midspan until failure occurred [Figure II.1(b)]. Steel stiffeners were placed at both supports to avoid premature local buckling. A load cell and a linear potentiometer were positioned at midspan of each beam to measure the load applied and corresponding deflection. Strain gages were bonded along the CFRP sheet at a spacing of 50 mm to monitor interfacial responses (the surface of the CFRP designated for the gages was flattened using sandpaper and cleaned with acetone), as shown in Figure II.1. Displacement-type strain transducers (position indicator gages or PI gages hereafter) having a gage length of 100 mm were installed at the upper and lower flanges. The loading rate applied was 1 mm/min. A computerized data acquisition system recorded all the responses, such as the load applied, displacement, and strains.

9.7 Fourier Transform Infrared Spectroscopy

Fourier transform infrared spectroscopy (FTIR) was conducted to investigate the consequence of the electrochemical reaction on the composition of the strengthening system. An attenuated total reflectance (ATR) technique was employed with a typical penetration depth of 2 mm and an incidence angle of 45° . Upon completion of the mechanical test described above, the failed CFRP sheet was cut to length, 20 mm by 30 mm, and exposed to infrared, as shown in Figure II.3. The absorbance of each specimen was detected within a range of 4000 cm^{-1} to 550 cm^{-1} , including an increment of 0.48 cm^{-1} . Response spectra were recorded to analyze the functional groups of the strengthening system subjected to electrochemical distress.

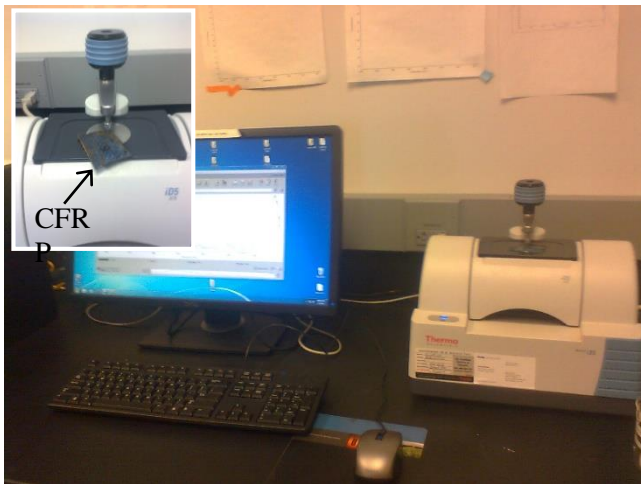


Figure II.3 Fourier transform infrared spectroscopy

10. TEST RESULTS

10.1 Propagation of Corrosion

A qualitative assessment of the strengthened beams subjected to the electrochemical reaction is provided in Figure II.4. It is apparent to note that corrosion has initiated near both ends of the beams at 12 hours, as shown in Figure II.4(a); however, the CFRP-strengthened region appeared to be intact. With a 36-hour increase in corrosion-processing time [Figure II.4(b)], dispersed surface-pitting was observed in the uncovered areas (i.e., outside the CFRP) of the beams, and partial brown rust was also noticed along the CFRP sheet. For the beams at 72 hours [Figure II.4(c)], the extent of corrosion became severe and rust formed in the steel spread widely and deeply with some localized crevice corrosion. The CFRP sheets were covered by rust-generated impurities; nonetheless, premature bond failure was not detected by visual inspection. Figure II.5 exhibits the corrosion-dependent properties of the strengthened beams. The measured surface area of the beams was virtually constant [Figure II.5(a)] even though an average drop of 2% was noticed when corrosion time increased from 0 hours to 72 hours. This observation implies that the surface area of the strengthened beams was not a contributing factor to the rate of corrosion. The average coefficient of variation (COV_{average} hereafter) of the surface area was approximately 6×10^{-4} . The loss of mass varied linearly with time, which can be categorized into three stages, as shown in Figure II.5(b): gradual (0 hours to 36 hours), steady (36 hours to 60 hours), and rapid (60 hours to 72 hours) increases. The first stage describes corrosion initiation and propagation due to irreversible oxidation. The second stage is concerned with serviceability based on the steady-state electrochemical reaction, while the last stage encompassed unstable dissolution. The transition from the second to the last stages might indicate serviceability concerns for the CFRP-strengthened steel beams. Figure II.5(c) reveals a decrease in electric potential, which can characterize the likelihood of corrosion. A slight downward gradient in potential was observed with an increase in time from 0 hours to 12 hours (0.04 V/hr on average), which implies that the strengthened beams experienced ion migration (from the anode to the cathode) and corrosion initiated accordingly. The decrease rate in potential became more pronounced between 12 hours and 24 hours (0.35 V/hr on average), beyond which a relatively stable decrease rate was observed up to 60 hours. The average potential at 72 hours was 8% compared with that of the 0-hour beams, while the average potential rate was 0.22 V/hr. This fact indicates that the potential difference between the anode and cathode became insignificant, thereby minimizing the flow of electric current or galvanic current between them. The variation of corrosion current density (i_{corr}) with time is provided in Figure II.5(d). Similar to the potential shown in Figure II.5(c), the current density was noticeably reduced up to 24 hours and exhibited a stable decrease rate until an exposure time of 72 hours was achieved. It is thought that the brown rust formed on the steel surface tended to impede the interaction between the anode and the electrolyte to a certain extent (i.e., less diffusion of iron ions), and hence the measured electric properties decreased with time.

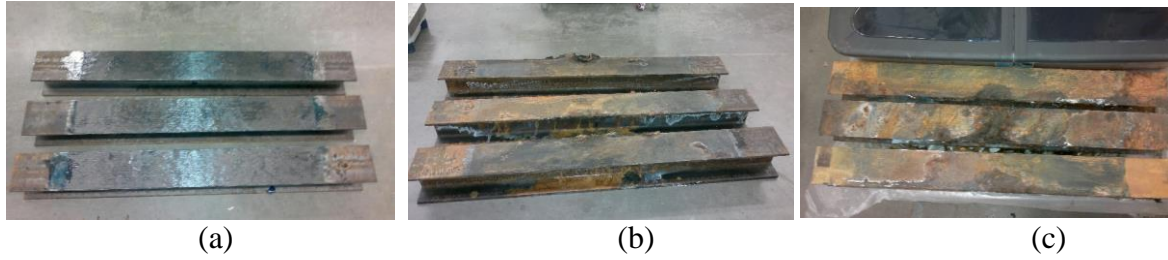


Figure II.4 Propagation of corrosion with time: (a) 12 hours; (b) 36 hours; (c) 72 hours

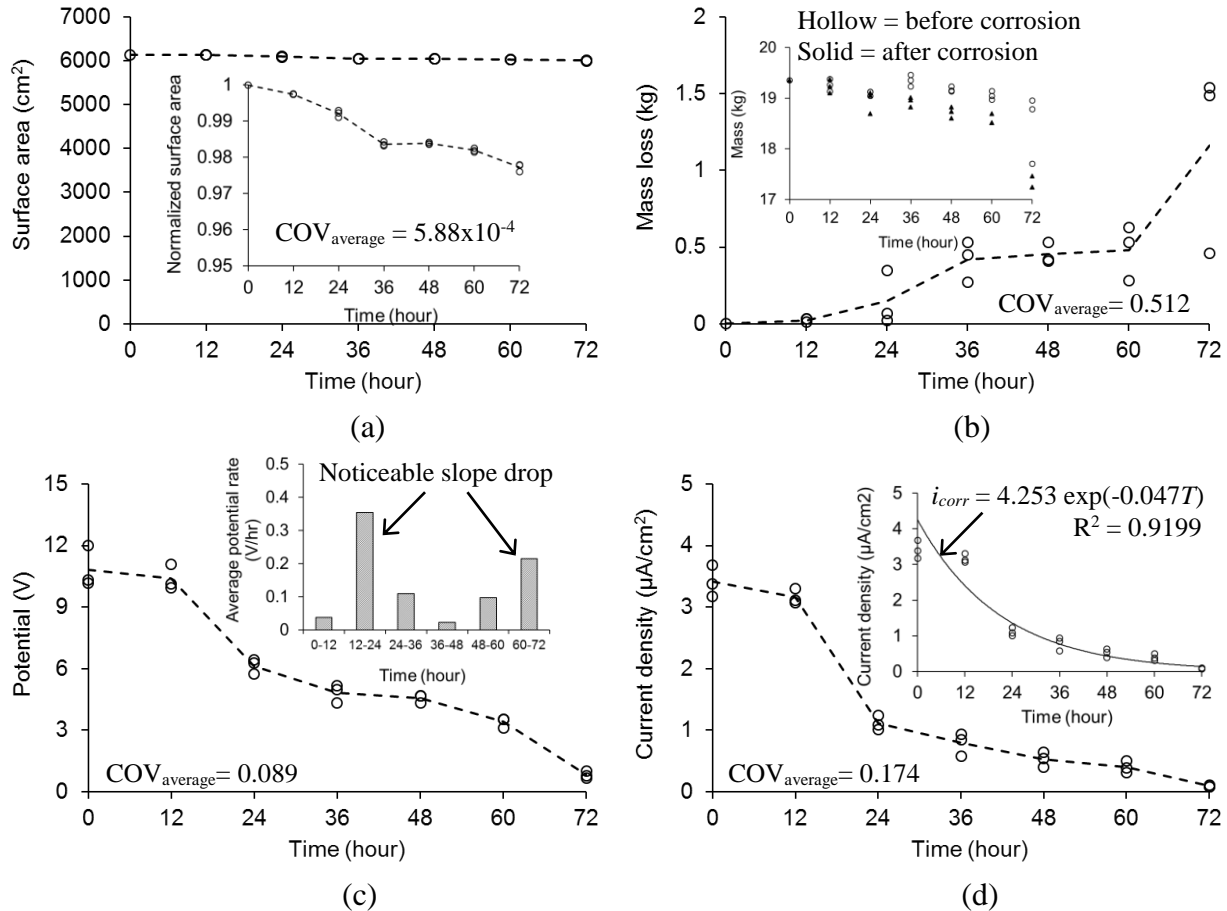


Figure II.5 Consequences of electrochemical reaction: (a) surface area; (b) mass loss; (c) electric potential; (d) corrosion current density

10.2 Corrosion Rate

Figure II.6 displays the corrosion rate of the strengthened beams determined by Faraday's law (Eq. II.1). The rate was maintained up to 12 hours with an average of 0.038 mm/year, followed by a noticeable drop until an exposure time of 72 hours was reached. This fact indicates that the development of corrosion was rapid at an early stage, while it had a propensity for slowing down when rust formed on the steel substrate due to less diffusion of iron ions, as explained earlier. The experimentally obtained average corrosion rate was 0.016 mm/year, which was close to the 10-year corrosion rate of ISO 9224 (ISO 2012) in the C3 category (medium corrosivity).

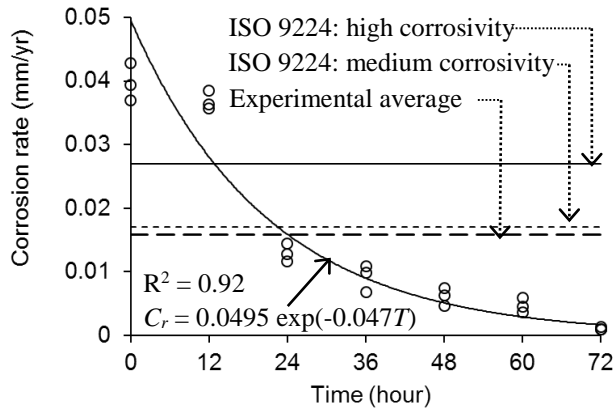


Figure II.6 Variation of corrosion rate based on Faraday’s law

10.3 Load-carrying Capacity

The failure load of the strengthened beams subjected to various levels of accelerated corrosion is provided in Figure II.7(a). Because of their relatively short span-length, lateral torsional buckling did not take place. The efficacy of CFRP-strengthening was significant without the occurrence of corrosion; in other words, the average load-carrying capacity of the strengthened beams at 0 hours was 66% greater than that of the un-strengthened case ($P_u = 37.9$ kN). The ultimate load of the beams was, however, reduced as the extent of corrosion augmented: a bilinear trend was observed before and after 36 hours of exposure according to the average line. The mean rates of load-drop from 0 hours to 36 hours and 48 hours to 72 hours were 0.40 kN/hr and 0.15 kN/hr, respectively. This indicates that the level of corrosion damage in the strengthened beams (specifically, damage of the CFRP-steel interface) had a transition period from an initiation-propagation phase to a steady-state-development phase. It was apparent that the bond between the CFRP and the steel substrate was influenced by the propagation of corrosion, thereby decreasing the effectiveness of CFRP-strengthening, as illustrated in Figure II.7(b), which is based on the strength efficiency factor Ω_{CFRP} (Eq. II.3). Such a long-term issue shall be considered when CFRP-strengthening for steel members is designed (further discussion is available in the Design Recommendations section). Figure II.8 depicts the load-displacement behavior of selected beams. The beams at 0 hours [Figure II.8(a)] showed an almost consistent response until their ultimate loads were reached at 62.9 kN on average (Table II.1), including yielding of the steel section followed by an abrupt load drop. The corrosion-damaged beams, on the other hand, exhibited somewhat scattered responses due to irregular corrosion damage along the CFRP-steel interface [Figure II.8(b) and (c)]. Nonetheless, the flexural stiffness of all the beams appeared to be more or less similar. Such a fact explains that synergetic damage (i.e., corrosion plus mechanical distress) on the interfacial bond was not obvious in a typical service stage beyond which the interfacial damage was accelerated by corrosion (lowering the load-carrying capacity of the beams).

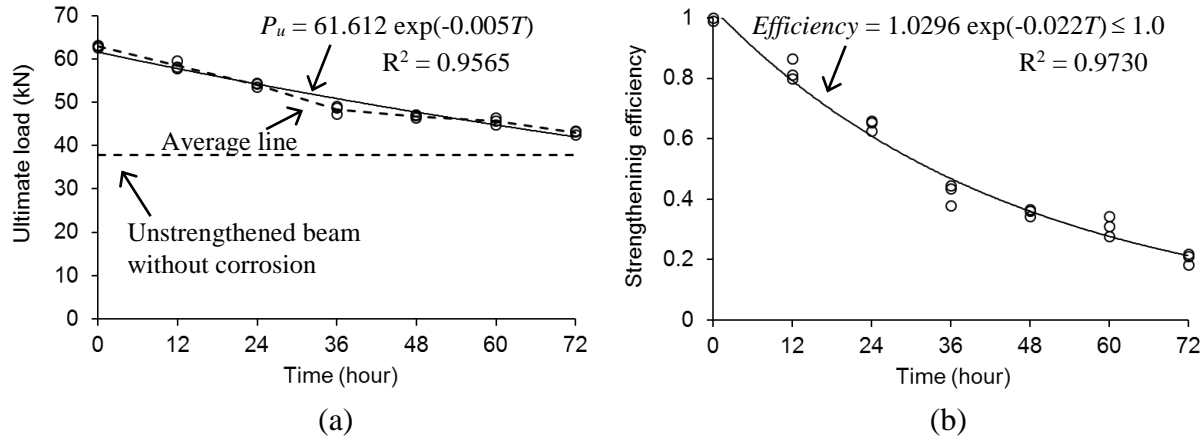


Figure II.7 Load-carrying capacity of the beams: (a) ultimate load; (b) efficiency of CFRP-strengthening

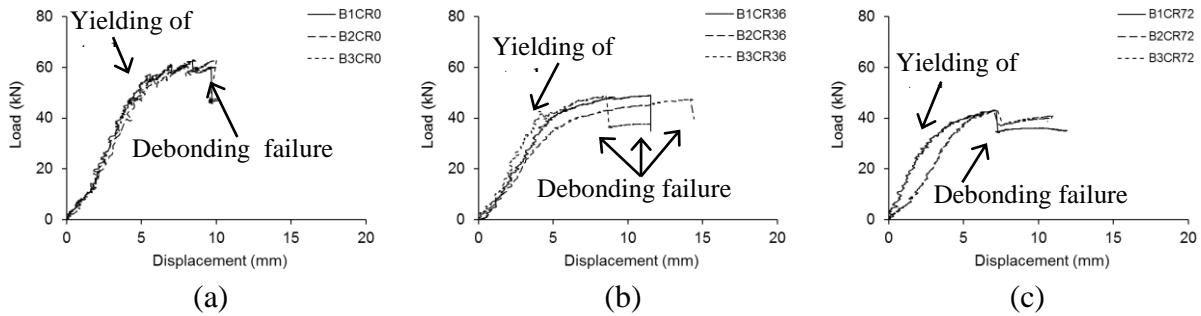


Figure II.8 Load-displacement behavior of CFRP-strengthened beams at various accelerated corrosion periods: (a) 0 hours; (b) 36 hours; (c) 72 hours

10.4 Failure Mode

The unstrengthened beam failed by ductile fracture in the vicinity of the midspan notch where stress singularity was associated, as illustrated in Figure II.9(a). The web-crack may be regarded as an intergranular fracture engaged with the slip of the lattice structure, accompanying gradual crack-tip plasticity (Cooke et al. 1975). All the strengthened beams demonstrated CFRP-debonding failure [Figure II.9(b)] because the interfacial stresses exceeded the adhesion capacity of the epoxy, irrespective of corrosion-damage level. More specifically, partial CFRP-debonding was first observed near the notch because of a geometric discontinuity associated with stress concentrations, and propagated along the bond-line with a further increase in load. Such a failure sequence resulted in an abrupt drop in the load and displacement behavior, as shown in Figure II.8. Once complete CFRP-debonding occurred, a sharp crack developed at the tip of the notch [inset of Figure II.9(b)] and the loading process was terminated; the local plasticity limit of the steel was reached. The secondary failure of these strengthened beams was a ductile fracture of the web as in the un-strengthened beam. Provided that the adhesion failure of the CFRP was the primary failure mode, the following can be postulated: i) corrosion developed along the steel substrate even though it was covered by an epoxy layer (chemical characterization of corrosion

damage will be discussed later) and ii) moisture diffusion into the micro-pores of the bonding agent was not a concern because cohesion failure (i.e., material level failure) was not noticed. It is worth noting that the debonding failure occurred after yielding of the steel section, as evidenced by Figure II.8, which means that the CFRP-strengthening system continuously carried the applied load even after some local debonding occurred near midspan. This observation is crucial from a practice standpoint because the efficacy of CFRP-strengthening can be preserved in spite of local damage that may be linked with fatigue-cracked steel members on site.



Figure II.9 Failure mode: (a) ductile fracture cracking; (b) CFRP-debonding

10.5 Strain Development

The load-strain behavior of the strengthened beams is given in Figure II.10. For the beam at 12 hours [Figure II.10(a)], all strains rapidly developed up to a load of 35 kN when local CFRP-debonding initiated at Gage 4 in the vicinity of the notch, followed by progressive debonding at Gages 5 and 6. Once the CFRP sheet was separated from the steel substrate, its strain development was unstable because of displacement incompatibility. With an increase in corrosion-exposure time, the debonding initiation load of the beams decreased. For instance, the debonding loads of the beams at 36 hours and 72 hours [Figure II.10(b) and (c)] were 63% and 76% lower than that of the beam at 12 hours [Figure II.10(a)], respectively. These observations confirm that corrosion damage has degraded the performance of the CFRP-steel interface. Other strengthened beams subjected to various corrosion-processing hours demonstrated similar responses (not shown for brevity). Figure II.11 presents strain profiles along the CFRP sheet of the beams at a typical interval of 25% of the ultimate loads (P_u). When the applied load level augmented, CFRP-debonding initiated and propagated along the bond-line supported by the increased strain values. Local damage (i.e., notch at midspan) attracted strain development, as mentioned earlier, and the usable CFRP strain at 100% P_u was reduced with an increase in corrosion damage. Another observation to note is that the breadth of CFRP-debonding was correlated with the degree of corrosion damage due to the deteriorated adhesion between the CFRP and the substrate.

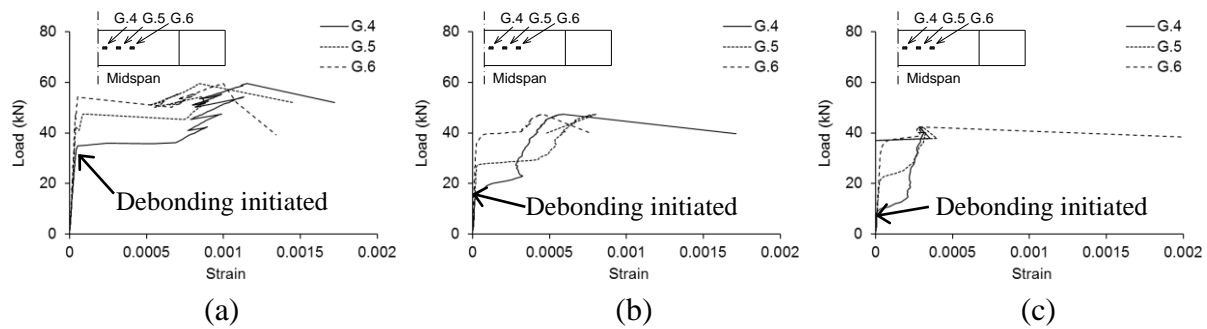


Figure II.10 CFRP strain development of corroded beams: (a) 12 hours; (b) 36 hours; (c) 72 hours

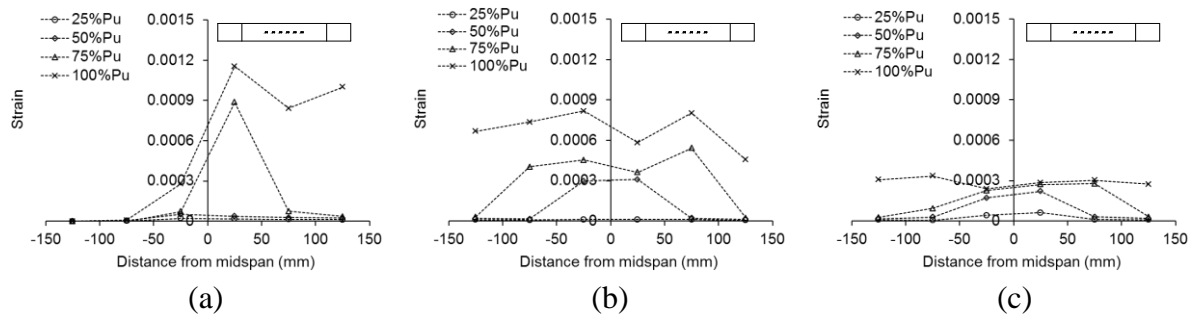


Figure II.11 Strain profile along the CFRP sheet: (a) 12 hours; (b) 36 hours; (c) 72 hours

10.6 Crack Mouth Opening Displacement

The crack mouth opening displacement (CMOD) of the beams measured by the lower-flange PI gage is depicted in Figure II.12. The CMOD of the 0-hour beam developed linearly within a service range, while load-softening accompanied by local spikes was noticed when a load level increased further. The presence of these local spikes denotes that the propagation of CFRP-debonding was not continuous along the interface so that a discrete debonding-progression pattern was recorded. It is interesting to note that the extent of such local spikes tended to diminish with an increase in corrosion-exposure hour, which indicates that the adhesion characteristics of the bonding agent were weakened (i.e., smooth debonding propagation). The slope of the load-CMOD behavior in an ascending branch tended to decay after 60 hours of corrosion exposure; in other words, the pseudo-confining or notch-closure effect by the bonded CFRP lessened because of the conditioned epoxy layer. The CMOD values at failure of the beams were reduced with increasing corrosion exposure. This can be explained by the fact that CFRP-debonding or interfacial failure was affected by the degree of the electrochemical reaction, and thus, the CMOD of the severely deteriorated beams did not sufficiently develop until their failure took place.

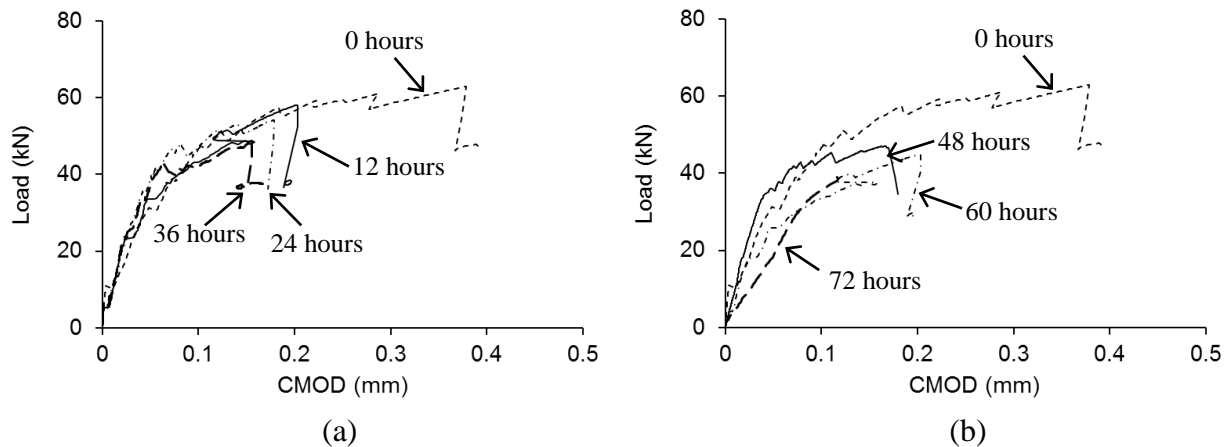


Figure II.12 Crack mouth opening displacement (CMOD) of strengthened beams: (a) up to 36 hours; (b) up to 72 hours

10.7 Chemical Characterization

Figure II.13 depicts the response spectra of selected CFRP specimens to characterize chemical changes caused by the corrosion exposure. A typical fingerprint region was noticed in between 550 cm^{-1} and 1500 cm^{-1} in conjunction with perplexing absorbance. The interpretation of the infrared spectra given below is available in organic chemistry texts such as McMurry (2012). For the 0-hr control specimen [Figure II.13(a)], the following was identified: The C-Br stretch of haloalkane and the $\text{-C}\equiv\text{C-H:C-H}$ bend of alkynes were first observed within wavenumber ranges from 550 cm^{-1} to 690 cm^{-1} and from 700 cm^{-1} to 610 cm^{-1} , respectively. The C-N stretch of the aliphatic amine functional group was noticed from 1020 cm^{-1} to 1250 cm^{-1} , followed by the N-O asymmetric stretch of nitro compounds in 1550 cm^{-1} to 1475 cm^{-1} . The last noticeable absorbance peak was the C-H stretch of the alkane functional group at a wavenumber of 2930 cm^{-1} . With an increase in corrosion exposure hour, the peak range from 550 cm^{-1} to 670 cm^{-1} arose; on the other hand, the peaks at a wavenumber-range from 1030 cm^{-1} to 1510 cm^{-1} decayed because most amine functional groups were eliminated due to the propagation of corrosion. The emerging peak at 3350 cm^{-1} of the corroded 48- and 72-hour specimens [Figure II.13(b) and (c)] illustrates a transition in functional group from alkane (C-H stretch) to amine (N-H stretch) by means of the electrochemical reaction. It may be reasonable to postulate that the specimens exposed to longer corrosion-simulation time included more active nitrogen atom responses than the un-corroded 0-hour specimen. The change of corrosion current density and corrosion rate [Figs. II.5(d) and 6] appears to have some relationship with the activation and deactivation of the aforementioned functional groups. Rigorous chemical analysis may be required to fully understand the exact structure alteration of the CFRP system, which is outside the scope of the present research.

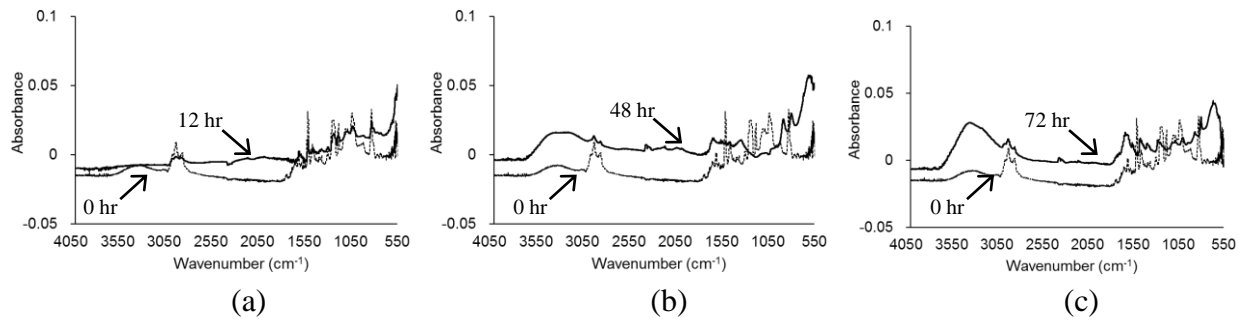


Figure II.13 Chemical response of the CFRP sheets: (a) 12 hours; (b) 48 hours; (c) 72 hours

11. DESIGN RECOMMENDATIONS

11.1 Equivalent Service Year

To develop realistic design recommendations, the accelerated corrosion hours discussed above and corresponding results may be converted to service years. The following formula proposed by Komp (1987) was adopted to estimate the in-situ corrosion rate of structural steel:

$$C_p = At^B \quad (\text{II.4})$$

where C_p is the corrosion progression in 10^{-6} m; t is the service time in years; and A and B are empirical constants dependent upon service condition ($A = 80.2$ and $B = 0.59$ were proposed for an urban environment by Albrecht and Naeemi [1984], which was developed by extensive examinations on the performance of constructed steel bridges in the United States). Figure II.14(a) exhibits the predicted corrosion progression of the steel beam up to 100 years with an assumption that CFRP-strengthening was not a major contributor to corrosion progression. The subsequent corrosion rate of the steel in mm/yr, $C_r(yr)$, is then followed by Figure II.14(b) and Eq. II.5, based on the corrosion progression of Figure 14(a) divided by service year:

$$C_r(yr) = 0.0802(yr)^{-0.41} \quad (\text{II.5})$$

The variation of the corrosion rate obtained in Figure II.6 resulted in Eq. II.6:

$$C_r(hr) = 0.0495e^{-0.047hr} \quad (\text{II.6})$$

Combining Eqs. II.5 and II.6 yields

$$hr_{eq}(hr) = -21.28 \ln(1.6202yr^{-0.41}) \geq 0 \quad (\text{II.7})$$

where $hr_{eq}(hr)$ is the equivalent laboratory hour hr to service year yr . It should be noted that a negative time cannot be predicted by Eq. II.7 due to the inequality condition and $hr_{eq}(hr) = 0$ along with newly constructed structural members (e.g., 1 or 2 years of service), indicating that corrosion has not occurred yet, which is valid in most existing steel bridges. Figure II.14(c) reveals the proposed parabola-like function of the equivalent service year against the accelerated laboratory time.

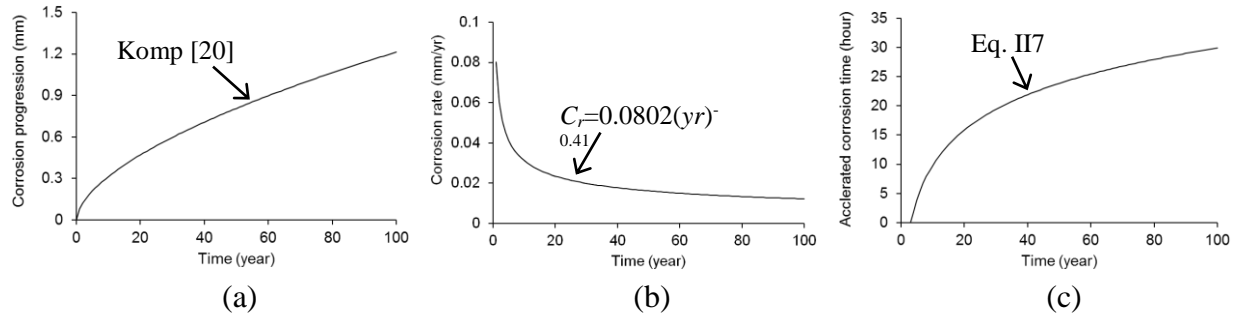


Figure II.14 Relationship between accelerated corrosion hour and equivalent service year:
 (a) predicted corrosion progression on site; (b) predicted corrosion rate on site;
 (c) proposed corrosion curve for time conversion

11.2 Bond Efficiency Factor

The degradation of the CFRP-steel interface due to corrosion should be taken into account when a strengthening design is conducted. The concept of a bond efficiency factor (κ_b) is proposed in Eq. II.8:

$$\kappa_b = \frac{C_{\text{corrosion-damage}}}{C_{\text{undamaged}}} \quad (\text{II.8})$$

where $C_{\text{corrosion-damage}}$ and $C_{\text{undamaged}}$ are the capacities of the CFRP-strengthened steel beam with and without corrosion damage, respectively. The deteriorated capacity of the strengthened beam due to corrosion may be determined by Eq. II.9 in conjunction with Figure II.7:

$$C_{\text{corrosion-damage}} = 61.612e^{-0.005hr} \quad (\text{II.9})$$

Figure II.15 presents the variation of the bond efficiency factor (κ_b) with respect to service time in years, which was acquired by the equivalent service hour (Eq. II.7) and the capacity change (Eq. II.9). For design convenience, the variable bond efficiency factors were simplified as listed in Table II.2.

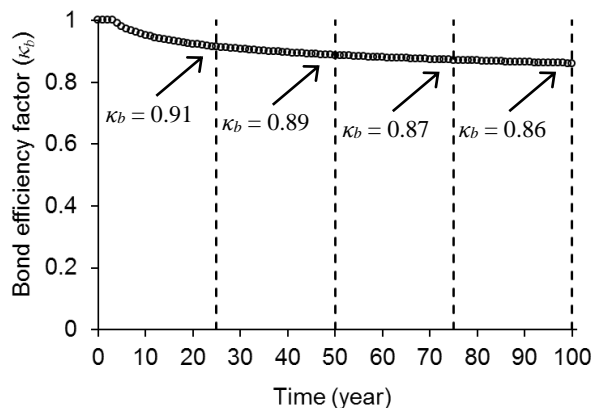


Figure II.15 Variation of bond efficiency factor

Table II.2 Proposed bond efficiency factor for design

Service time	Bond efficiency factor (κ_b)
0 to 50 years	0.90
51 years to 100 years	0.85

12. SUMMARY AND CONCLUSIONS

This paper has dealt with an experimental program examining the effect of an electrochemical reaction on the performance of CFRP-strengthened steel beams. An accelerated corrosion protocol was implemented and subsequent test data were obtained. The consequence of corrosion damage was physically and chemically characterized, including electric potential, mass loss, corrosion current density, corrosion rate, load-carrying capacity, interfacial strain development, failure mode, and infrared spectroscopy. It is worthwhile to note that protective layers, such as a primer, may be placed between the steel substrate and the CFRP to improve durability of the CFRP-steel interface. Design recommendations were proposed to facilitate the use of CFRP-strengthening techniques based on the fact that the accelerated test protocol reasonably represented the deterioration mechanism of constructed steel bridges; this is a typical assumption in durability research, and thus, the model was intended to guide practitioners rather than to accurately quantify the extent of corrosion damage. The following conclusions are drawn:

- With an increase in electrochemical reaction time, deterioration was dispersed along the beams. Surface-pitting and localized crevice-corrosion were noticed; however, premature CFRP-debonding was not observed. The surface area of the corroded beams was not a major parameter to consider when quantifying the degree of corrosion damage. The service limit state of the strengthened beams appeared to be correlated with the loss of mass.
- As corrosion propagated, the flow of electric current decreased and the surface rust impeded the interaction between the anode and electrolyte so that the diffusion of iron ions was reduced. The development of corrosion was active at an early electrochemical stage; however, it tended to be stable with time. An average corrosion rate of 0.016 mm/year is recommendable for the steel beams strengthened with CFRP sheets in corrosive service environments.
- The strength reduction of the beams was classified into two phases: initiation-propagation and steady-state. Although the load-carrying capacity of the strengthened beams was affected by the extent of corrosion damage, their flexural stiffness at service and individual failure mode (CFRP-debonding) were independent of damage levels. Localized CFRP-debonding prior to noticeable propagation was not a critical factor influencing the performance of the beams.
- In accordance with observations on CMOD, the pattern of debonding along the CFRP was shifted from discrete-discontinuous to smooth progression. The pseudo-confining effect of the bonded CFRP dwindled as the electrochemical reaction became active, in particular after 60 hours of accelerated corrosion exposure.
- The initiation and propagation of corrosion altered the functional groups of the strengthening system from a chemistry perspective. The response of nitrogen atoms became more pronounced as the degree of the electrochemical reaction augmented.
- The bond efficiency factors proposed were 0.90 and 0.85 for service time up to and beyond 50 years, respectively, which can be multiplied by the nominal capacity of an undamaged CFRP-strengthened beam when a design is conducted.

13. REFERENCES

- Ahmad, Z. 2006. *Principles of corrosion engineering and corrosion control*, Butterworth Heinemann, Oxford, UK.
- Albrecht, P., and Naeemi, A.H. 1984. *Performance of weathering steel in bridges*, National Cooperative Highway Research Program (NCHRP-272), Transportation Research Board, Washington, D.C.
- Albrecht, P., and Hall, T.T, 2003. "Atmospheric corrosion resistance of structural steels," *Journal of Materials in Civil Engineering*, 15(1), 2-24.
- ASTM. 2011. *Standard practice for preparing, cleaning, and evaluating corrosion test specimens* (ASTM G01-03), American Society for Testing and Materials, West Conshohocken, PA.
- ASTM. 2011. *Standard specification for structural steel shapes* (ASTM A992-11), American Society for Testing and Materials, West Conshohocken, PA.
- Cooke, R.J., Irving, P.E., Booth, G.S., and Beevers, C.J. 1975. "The slow fatigue crack growth and threshold behaviour of a medium carbon alloy steel in air and vacuum," *Engineering Fracture Mechanics*, 7, 69-77.
- Dawood, M., and Rizkalla, S. 2010. "Environmental durability of a CFRP system for strengthening steel structures," *Construction and Building Materials*, 24(9), 1682-1689.
- Doyle, G., and Pethrick, R.A. 2009. "Environmental effects on the ageing of epoxy adhesive joints," *International Journal of Adhesion and Adhesives*, 29, 77-90.
- Gholami, M., Sam, A.R.M., Yatim, J.N., and Tahir, M.M. 2013. "A review on steel/CFRP strengthening systems focusing environmental performance," *Construction and Building Materials*, 47, 301-310.
- Grant, L.D.R., Adams, R.D., da Silva, L.F.M. 2009. "Effect of the temperature on the strength of adhesively single lap and T joints for the automotive industry," *International Journal of Adhesion and Adhesives*, 29, 535-542.
- Hollaway, L.C., and Cadei, J. 2002. "Progress in the technique of upgrading metallic structures with advanced polymer composites," *Progress in Structural Engineering and Materials*, 4, 131-148.
- ISO. 2012. *Corrosion of metals and alloys* (ISO 9224), International Organization for Standardization, Geneva, Switzerland.
- Komp, M.E. 1987. "Atmospheric corrosion ratings of weathering steels - calculation and significance," *Material Performance*, 26(7), 42-44.

McMurry, J. 2012. *Organic chemistry, 8th edition*, Cengage Learning, Boston, MA.

Nakamura, H., Jiang, W., Suzuki, H., Maeda, K., and Irube, T. 2009. "Experimental study on repair of fatigue cracks at welded web gusset joint using CFRP strips," *Thin-walled Structures*, 47, 1059-1068.

Nozaka, K., Shield, C.K., and Hajjar, J.F. 2005. "Effective bond length of carbon fiber reinforced polymer strips bonded to fatigued steel bridge I girders," *Journal of Bridge Engineering*, 10(2), 195-205.

O'Connor, A.J., Sheils, E., Breysse, D., and Schoefs, F. 2013. "Markovian bridge maintenance planning incorporating corrosion initiation and nonlinear deterioration," *Journal of Bridge Engineering*, 18(3), 189-199.

Rahgozar, R. 2009. "Remaining capacity assessment of corrosion damaged beams using minimum curves," *Journal of Constructional Steel Research*, 65, 299-307.

Shaat, A., and Fam, A. 2008. "Repair of cracked steel girders connected to concrete slabs using carbon-fiber-reinforced polymer sheets," *Journal of Composites for Construction*, 12(6), 650-659.

Teng, J.G., Yu, T., and Fernando, D. 2012. "Strengthening of steel structures with fiber-reinforced polymer composites," *Journal of Construction Steel Research*, 78, 131-143.

Zhao, X.-L., Bai, Y., Al-Mahaidi, and Rizkalla, S. 2014. "Effect of dynamic loading and environmental conditions on the bond between CFRP and steel: state-of-the-art review," *Journal of Composites for Construction*, 18(3), A4013005-1.